Distortion-resistant and locking-free eight-node elements effectively capturing the edge effects of Mindlin-Reissner plates

Journal:	*Engineering Computations*
Manuscript ID	EC-04-2016-0143.R1
Manuscript Type:	Research Article
Keywords:	finite element methods, hybrid displacement function element, analytical trial function, edge effect, plate bending

Distortion-resistant and locking-free eight-node elements effectively capturing the edge effects of Mindlin-Reissner plates

Abstract

Purpose—A simple shape-free high-order hybrid displacement function element method is presented for precise bending analyses of Mindlin-Reissner plates. Three distortion-resistant and locking-free eight-node plate elements are proposed by utilizing this method.

Design/methodology/approach—This method is based on the principle of minimum complementary energy, in which the trial functions for resultant fields are derived from two displacement functions, F and f, and satisfy all governing equations. Meanwhile, the element boundary displacements are determined by the locking-free arbitrary order Timoshenko's beam functions. Then, three locking-free 8-node, 24-DOF quadrilateral plate bending elements, HDF-P8-23β for general cases, HDF-P8-SS1 for edge effects along soft simply supported (SS1) boundary, and HDF-P8-FREE for edge effects along free boundary, are formulated.

Findings—The proposed elements can pass all patch tests, exhibit excellent convergence and possess superior precision when compared to all other existing 8-node models, and can still provide good and stable results even when extremely coarse and distorted meshes are used. They can also effectively solve the edge effect by accurately capturing the peak value and the dramatical variations of resultants near the SS1 and Free boundaries. The proposed 8-node models possess the potential in the engineering application and could be easily integrated into the commercial software.

Originality/value—This work presents a new scheme, which can take the advantages of both analytical and discrete methods, to develop high-order mesh-distortion resistant Mindlin-Reissner plate bending elements.

Keywords finite element methods; hybrid displacement function element; analytical trial function; edge effect; plate bending

Paper type Research paper

1. Introduction

The availability of simple, efficient and reliable elements for thin and thick plates represents one of the main features of all finite element computer program libraries for structural analysis. To date, considerable research efforts have been made to develop various plate bending elements (Bathe 1996; Cen and Shang 2015; Long *et al.* 2009; Zienkiewicz and Taylor 2000), in which many models are based on Mindlin–Reissner plate theory (Mindlin 1951; Reissner 1945). Unlike the thin plate theory which requires C_1 continuity between the displacement fields of two adjacent elements, Mindlin-Reissner plate theory only requires C_0 continuity and can be used for both thin and moderately thick plates (Crisfield 1984).

Most conventional Mindlin-Reissner plate elements are displacement-based models and generally perform well in moderately thick-plate applications. However, when the span-to-thickness ratio of the plate becomes very large, their performances often become over stiff, so they are not reliable for thin-plate cases. This numerical difficulty is known as the transverse shear locking caused by false shear strains. During the history of finite element method, many investigators have proposed recognized treatments on shear locking, including the classical reduced (Zienkiewicz *et al.* 1971) and selective reduced integral schemes (Hughes *et al.* 1977), the stabilization procedure for reduced integral (Belytschko *et al.* 1981; Belytschko and Tsay 1983), the mixed interpolated tensorial components (MITC) techniques (Bathe and Dvorkin 1985,1986), the substitute shear strain methods (Hinton and Huang 1986; Onate *et al.* 1992), the mixed element method derived from the modified Hellinger-Reissner principle (Lee and Wong 1982), the linked interpolation schemes (Taylor and Auricchio 1993; Zienkiewicz *et al.* 1993), the discrete shear constraint methods (Batoz and Lardeur 1989; Katili 1993), the hybrid-mixed variational approach (Ayad *et al.* 1998; Ayad and Rigolot 2002), the enhanced displacement interpolation (Ibrahimbegović 1993), the improved interpolation based on locking-free Timoshenko's beam formulae (Chen and Cheung 2000; Soh *et al.* 1999a,1999b,2001), the generalized conforming Mindlin-Reissner plate element (Cen *et al.* 2006) based on the quadrilateral area coordinates (Long *et al.* 2009; Long *et al.* 2009), the smoothed FEM(SFEM) (Nguyen-Thoi *et al.* 2012; Nguyen-Xuan *et al.* 2008;2009), and so on (Cen *et al.* 2002; Falsone and Settineri 2012; Hansbo *et al.* 2011; Hu *et al.* 2010; Jin *et al.* 1993; Jin and Qin 1995; Jirousek *et al.* 1995a,1995b; Nguyen-Thoi *et al.* 2011; Petrolito 1990,1996; Rezaiee-Pajand and Karkon 2012; Ribaric and Jelenic 2012). On the other hand, high-order elements usually have better precisions and exhibit better performance for thin plate cases. So, many attempts have also been devoted to construct high-order models free of shear locking. Ahmad *et al.* (1970) applied Mindlin-Reissner plate theory in the degenerated shell approach and developed an 8-node isoparametric element; Crisfield (1984) developed a quadratic element using shear constraints; Spilker *et al.* (1980,1982) proposed 8-node hybrid-stress elements for analysis of thin and moderately thick plates; Hughes and Cohen (1978) presented a so-called "heterosis" element which utilized an 8-node interpolation for rotations and 9-node interpolation for deflections; Kant *et al.* (1982) proposed an element based on a higher-order displacement mode and a three-dimensional state of stress and strain;

Hinton and Huang (1986) developed a family of elements, including 8-,9-,12- and 16-node ones, with substitute strain fields; Donea and Lamain (1987) provided a modified representation of transverse shear component in 8-node and 9-node quadrilateral plate elements; Polit *et al.* (1994) proposed an 8-node quadrilateral element, in which each monomial term of the interpolation functions for the normal rotations is matched by the derivatives of its corresponding deflection; Zhang and Kuang (2007) developed a new 8-node Reissner–Mindlin plate element with a special interpolation within the element, this special interpolation is an extension of the element boundary interpolation that employs Timoshenko beam function for the boundary segment interpolation; Dhananjaya *et al* (2009) adopted the integrated force method to construct an 8-node serendipity quadrilateral thin-thick plate bending element (MQP8); Li *et al* (2015) presented an 8-node quadrilateral assumed stress hybrid Mindlin plate element with 39 unknown parameters. These efforts more or less improved the element resistance to shear locking problem

In addition to above shear locking problem, how to obtain good resultant/stress solutions is another problem that should be concerned about. For a Mindlin-Reissner plate, its rotations and stress resultants may vary sharply in a narrow region at the vicinity of certain types of boundary conditions. This is so-called the edge effect or the boundary layer effect, and represents another interesting and troublesome numerical challenge in Mindlin-Reissner plate theory (Arnold and Falk 1989). However, aforementioned efforts mainly concentrate on the shear-locking problem, few solution strategies have been considered for solving this difficulty. Although the edge effect does not impose great influences on the entire structure, it will make the numerical analysis more complicated. Some analytical, semi-analytical and discrete methods have been proposed to conquer this challenging topic (Arnold and Falk 1990; Babuška and Scapolla 1989; Briassoulis 1993a,1993b; Haggblad and Bathe 1990; Hinton *et al.* 1995; Kant and Gadgil 2002; Kant and Hinton 1983; Rao *et al.* 1992; Wang *et al.* 2002; Ye and Yuan 2002; Yuan 1993; Yuan *et al.* 1998), but few finite element models can easily and accurately predict the distributions of the resultants near the plate boundaries when edge effect takes place.

Besides good behaviors in dealing with shear locking and edge effect problems, an ideal plate bending element should have following features: i) no any adjusted factor existing in its formulations; ii) high tolerance to various mesh distortions; and iii) high-precision results for stress/resultant solutions as well as the displacements. Recently, in order to develop plane

quadrilateral elements immune to mesh distortions, Fu *et al.* (2010) and Cen *et al.* (2011a,2011b,2011c) proposed a simple hybrid stress-function (HSF) element method, in which the trial functions for stress fields are the analytical solutions of the stress function ϕ. Inheriting from this technique, Cen *et al.* (2014) and Shang *et al.* (2015) established a simple hybrid displacement-function (HDF) element method for constructing Mindlin-Reissner plate bending elements, in which the trial functions for resultant fields are derived from two displacement functions, F and f (Hu 1984), and satisfy all governing equations. Then, a robust shape-free 4-node, 12-DOF quadrilateral element HDF-P4-11β for general cases, two shape-free 4-node, 12-DOF quadrilateral elements HDF-P4-Free and HDF-P4-SS1 for solving edge effects along free and soft simply supported (SS1) boundaries, respectively, were successfully developed. Numerical examples proved that these new models possess outstanding performances among all existing 4-node models, no matter for conventional problems, or for edge effects.

Actually, above hybrid displacement function element method can be simply extended to construct higher-order elements, so that more precise results for both displacements and resultants, especially for the resultant distributions with edge effects, can be obtained using fewer elements. In this paper, three 8-node, 24-DOF quadrilateral Mindlin-Reissner plate bending elements for different purpose are presented. For general situation, twenty-three sets of the resultant components derived from the displacement function F and satisfying all governing equations are taken as the trial functions for resultant fields. Meanwhile, the element boundary displacements and shear strains are determined by the locking-free arbitrary order Timoshenko's beam functions (Jelenic and Papa 2011). Then, an 8-node, 24-DOF quadrilateral plate bending element, HDF-P8-23β, is firstly formulated by the principle of minimum complementary energy. For special situation consisting of the edge effect or the boundary layer effect (SS1 and FREE types), the additional displacement function f related to the edge effect is considered. Then, two new 8-node, 24-DOF quadrilateral elements, denoted by HDF-P8-SS1 and HDF-P8-FREE, are also constructed. The proposed elements pass all patch tests, exhibit excellent convergence and possess superior precision when compared to other existing 8-node models, and can still provide good and stable results even when extremely coarse and distorted meshes are used. It can also effectively solve the edge effect by accurately capturing the peak value and the dramatical variations of resultants near the SS1 and Free boundaries. The proposed 8-node models possess the potential in

the engineering application and could be easily integrated into the commercial software.

2. The arbitrary order Timoshenko's beam functions

For a robust Mindlin-Reissner plate bending element, it is necessary to eliminate the phenomenon of shear locking which induces an over stiff problem as the plate becomes progressively thinner. So, how to determine rational displacement modes and shear strains along element edges becomes a key technique for many existing models. In the formulations of some low-order plate elements, a set of locking-free functions for 2-node Timoshenko beam have been successfully applied (Cen *et al.* 2002,2006,2014; Chen and Cheung 2000; Soh *et al.* 1999a,1999b,2001; Shang *et al.* 2015). Recently, Jelenic and Papa (2011) presented a set of new arbitrary order Timoshenko beam functions. These functions are given by:

$$w=\sum_{i=1}^{n} I_i w_i - \frac{L}{n}\prod_{j=1}^{n} N_j \sum_{i=1}^{n}(-1)^{i-1}\binom{n-1}{i-1}\psi_i\,,\quad \psi=\sum_{i=1}^{n} I_i\psi_i\,, \tag{1}$$

where L is the beam length; w_i and ψ_i (i=1~n) are the nodal displacements and the rotations at the nth nodes equidistantly located between the beam ends; I_i (i=1~n) are the standard Lagrange polynomials of order n−1;

$$\begin{cases} \text{for } j=1, & N_j=\dfrac{r}{L} \\ \text{else,} & N_j=1-\dfrac{(n-1)\,r}{(j-1)\,L} \end{cases}, \tag{2}$$

in which r is the length along the beam from the starting point. For an 8-node quadrilateral element, any quadrilateral side can be treated as a 3-node Timoshenko beam element as given in Figure 1. Then, the displacement and rotations can be obtained:

$$\bar{w}=I_a w_i + I_b w_j + I_c w_k - I_0[(\psi_{xi}+\psi_{xj}-2\psi_{xk})l_x^* - (\psi_{yi}+\psi_{yj}-2\psi_{yk})l_y^*], \tag{3}$$

$$\bar{\psi}_x = I_a\psi_{xi} + I_b\psi_{xj} + I_c\psi_{xk}\,,\quad \bar{\psi}_y = I_a\psi_{yi} + I_b\psi_{yj} + I_c\psi_{yk}\,, \tag{4}$$

with

$$\begin{cases} L_1 = 1-s, L_2 = s, I_a = L_1(2L_1-1), I_b = L_2(2L_2-1), I_c = 4L_1L_2, I_0 = \dfrac{L_1L_2(L_2-L_1)}{3} \\ l_x^* = (4s-3)x_i + (4s-1)x_j + (4-8s)x_k, l_y^* = -(4s-3)y_i - (4s-1)y_j - (4-8s)y_k \\ l_x = \dfrac{-l_y^*}{(l_x^{*2}+l_y^{*2})^{\frac{1}{2}}}, l_y = \dfrac{-l_x^*}{(l_x^{*2}+l_y^{*2})^{\frac{1}{2}}} \end{cases}, \quad (5)$$

in which $s=r/L$ is the local coordinate along the beam (varies from 0 to 1). One should be noticed here that the formulations are valid for curved boundaries because at different points along the boundaries different tangent directions and outer normal directions could be derived by applying differential method.

Thus, the displacement components $\bar{\mathbf{u}}$ along the *i*-*j*-*k* boundary can be written as

$$\bar{\mathbf{u}}_{ijk} = \begin{Bmatrix} \bar{w} \\ \bar{\psi}_x \\ \bar{\psi}_y \end{Bmatrix} = \begin{bmatrix} I_a & -I_0 l_x^* & I_0 l_y^* & I_b & -I_0 l_x^* & I_0 l_y^* & I_c & 2I_0 l_x^* & -2I_0 l_y^* \\ 0 & I_a & 0 & 0 & I_b & 0 & 0 & I_c & 0 \\ 0 & 0 & I_a & 0 & 0 & I_b & 0 & 0 & I_c \end{bmatrix} \mathbf{q}_{ijk} = \mathbf{L}_{abc}\mathbf{q}_{ijk}, \quad (6)$$

where

$$\mathbf{q}_{ijk} = \begin{bmatrix} \mathbf{q}_i & \mathbf{q}_j & \mathbf{q}_k \end{bmatrix}^{\mathrm{T}}, \ \mathbf{q}_m = \begin{bmatrix} w_m & \psi_{xm} & \psi_{ym} \end{bmatrix}^{\mathrm{T}} (m = i, j, k) \quad (7)$$

3. The General formulations of the HDF elements

In element level, the finite element equations can be written as:

$$\mathbf{K}^e\mathbf{q}^e = \mathbf{P}_q^e, \quad (8)$$

in which $\mathbf{K}^e$ is the element stiffness matrix; $\mathbf{q}^e$ is the element nodal displacement vector; and $\mathbf{P}_q^e$ is the element nodal equivalent load vector caused by the distributed transverse load q.

Following the construction procedure of the hybrid-displacement function elements (Cen *et al.* 2014), the element stiffness matrix of the Mindlin-Reissner plates can be obtained:

$$\mathbf{K}^e = \mathbf{H}^{\mathrm{T}}\mathbf{M}^{-1}\mathbf{H}; \quad (9)$$

$$\mathbf{P}_q^e = \mathbf{V}^{\mathrm{T}} - \mathbf{H}^{\mathrm{T}}\mathbf{M}^{-1}\mathbf{M}^*. \quad (10)$$

where

$$\mathbf{M}=\iint_{A^e}\hat{\mathbf{S}}^{\mathrm{T}}\mathbf{C}\hat{\mathbf{S}}\mathrm{d}x\mathrm{d}y\,,\quad \mathbf{M}^{*}=\iint_{A^e}\hat{\mathbf{S}}^{\mathrm{T}}\mathbf{C}\mathbf{R}^{*}\mathrm{d}x\mathrm{d}y\,,\quad \mathbf{Q}=\iint_{A^e}\mathbf{R}^{*\mathrm{T}}\mathbf{C}\mathbf{R}^{*}\mathrm{d}x\mathrm{d}y\,, \tag{11}$$

$$\mathbf{H}=\int_{S^e}\hat{\mathbf{S}}^{\mathrm{T}}\mathbf{L}^{\mathrm{T}}\bar{\mathbf{N}}\big|_{\Gamma}\,\mathrm{d}s\,,\quad \mathbf{V}=\int_{S^e}\mathbf{R}^{*\mathrm{T}}\mathbf{L}^{\mathrm{T}}\bar{\mathbf{N}}\big|_{\Gamma}\,\mathrm{d}s\,. \tag{12}$$

In above equations, $\hat{\mathbf{S}}$ represents the general solution part; $\mathbf{R}^{*}$ represents the corresponding particular solutions of the resultant forces (for different distributions of the transverse load q, $\mathbf{R}^{*}$ is also different); $\mathbf{C}$ is the flexibility matrix:

$$\mathbf{C}=\begin{bmatrix}\frac{1}{D(1-\mu^2)} & \frac{-\mu}{D(1-\mu^2)} & 0 & 0 & 0\\ \frac{-\mu}{D(1-\mu^2)} & \frac{1}{D(1-\mu^2)} & 0 & 0 & 0\\ 0 & 0 & \frac{2}{D(1-\mu)} & 0 & 0\\ 0 & 0 & 0 & \frac{1}{C} & 0\\ 0 & 0 & 0 & 0 & \frac{1}{C}\end{bmatrix}, \tag{13}$$

with Poisson's ratio μ and the bending stiffness D of the plate; $\mathbf{L}$ denotes the matrix of the direction cosines for element boundaries:

$$\mathbf{L}=\begin{bmatrix}l_x^2 & l_y^2 & 2l_xl_y & 0 & 0\\ -l_xl_y & l_xl_y & l_x^2-l_y^2 & 0 & 0\\ 0 & 0 & 0 & -l_x & -l_y\end{bmatrix}, \tag{14}$$

where l_x and l_y denote the direction cosines of outer normal of the element boundary; $\bar{\mathbf{N}}\big|_{\Gamma}$ is the interpolation matrix for boundary displacements, and has different values along each element edge. The components of $\bar{\mathbf{N}}\big|_{\Gamma}$ are derived from the formulae of the arbitrary order Timoshenko's beam functions given in last section (Jelenic and Papa 2011), and their detailed expressions are given in Appendix.

According to Reference (Hu 1984), the solutions of rotations ψ_x, ψ_y and deflection w for a Mindlin-Reissner plate can be expressed by :

$$\psi_x=\frac{\partial F}{\partial x}+\frac{\partial f}{\partial y},\psi_y=\frac{\partial F}{\partial y}-\frac{\partial f}{\partial x},w=F-\frac{D}{C}\nabla^2F\,, \tag{15}$$

with

$$D=\frac{Eh^3}{12\left(1-\mu^2\right)},\quad C=\frac{5}{6}Gh\,, \tag{16}$$

where h is the plate thickness; E is Young's modulus; $G=E/[2(1+\mu)]$ is shear modulus; F and f in

Equation (15) are two displacement functions and satisfy following equations

$$D\nabla^2\nabla^2 F = q\,, \tag{17}$$

$$\frac{1}{2}(1-\mu)D\nabla^2 f - Cf = 0\,, \tag{18}$$

in which q is the distributed transverse load. From Equations (9) to (12), the key point for formulating the HDF elements is to define the general solution part $\hat{\mathbf{S}}$ and the corresponding particular solutions $\mathbf{R}^*$ of the resultant forces which can be derived from the two displacement function F and f.

3.1. Formulations of element HDF-P8-23β (without edge effects)

Figure 2 shows an 8-node quadrilateral plate bending element. In normal situation, the first displacement function F in Equation (17) is capable of reflecting the deformation of a Mindlin-Reissner plate. Based on the derivations given by Cen *et al.* (2014), the trial functions for the resultant forces without edge effects can be expressed by the displacement function F as:

$$\mathbf{R}_{\text{normal}} = \begin{Bmatrix} M_x \\ M_y \\ M_{xy} \\ T_x \\ T_y \end{Bmatrix} = \mathbf{R}^0 + \mathbf{R}^* = \sum_{i=1}^{k} \mathbf{R}_i^0 \beta_i + \mathbf{R}^* = \hat{\mathbf{S}}\boldsymbol{\beta} + \mathbf{R}^*\,, \tag{19}$$

with

$$\mathbf{R}^0 = \sum_{i=1}^{k} \mathbf{R}_i^0 \beta_i\,,\quad \mathbf{R}^0 = \begin{Bmatrix} M_x^0 \\ M_y^0 \\ M_{xy}^0 \\ T_x^0 \\ T_y^0 \end{Bmatrix} = \begin{Bmatrix} \dfrac{\partial^2 F^0}{\partial x^2} + \mu\dfrac{\partial^2 F^0}{\partial y^2} \\ \dfrac{\partial^2 F^0}{\partial y^2} + \mu\dfrac{\partial^2 F^0}{\partial x^2} \\ (1-\mu)\dfrac{\partial^2 F^0}{\partial x \partial y} \\ \dfrac{\partial}{\partial x}(\nabla^2 F^0) \\ \dfrac{\partial}{\partial y}(\nabla^2 F^0) \end{Bmatrix},\ \mathbf{R}^* = \begin{Bmatrix} M_x^* \\ M_y^* \\ M_{xy}^* \\ T_x^* \\ T_y^* \end{Bmatrix} = \begin{Bmatrix} -\dfrac{q}{4}(x^2 + \mu y^2) \\ -\dfrac{q}{4}(\mu x^2 + y^2) \\ 0 \\ -\dfrac{q}{2}x \\ -\dfrac{q}{2}y \end{Bmatrix}, \tag{20}$$

$$\hat{\mathbf{S}} = \begin{bmatrix} \mathbf{R}_1^0 & \mathbf{R}_2^0 & \cdots & \mathbf{R}_k^0 \end{bmatrix}_{5\times k}, \tag{21}$$

where β_i (i=1~k) are k unknown coefficients; F_i^0 are the (i=1~k) are k analytical solutions (in Cartesian coordinates) of F^0 which generated from the homogeneous equation of Equation (17).

The first twenty-three analytical solutions of F^0 (seventh-order completed in Cartesian coordinates) and related resultant solutions are given in Table I. Meanwhile, $\mathbf{R}^*$ represents the corresponding particular solutions of the resultant forces under uniformly distributed transverse load q (for transverse load q with different distributions, $\mathbf{R}^*$ is also different).

After substituting the corresponding $\hat{\mathbf{S}}$ and $\mathbf{R}^*$ into Equations (9) to (12), a new 8-node quadrilateral plate bending element is constructed. This element is denoted by HDF-P8-23β (without edge effects), and it is very easy to be integrated into the standard framework of finite element programs.

3.2. Formulations of elements HDF-P8-SS1 (with SS1 edge effects) and HDF-P8-FREE(with free edge effects)

When the edge effect is taken into consideration, the second displacement function f has significant effect on the performance of the elements. At the vicinity of certain types of boundary conditions, it has a significant value near the plate boundaries, but can be ignored in other area (Shang *et al.* 2015).

After considering the second displacement function f, the resultant forces with edge effects can be assumed as:

$$\mathbf{R}_{\text{edge}}=\begin{Bmatrix} M_x \\ M_y \\ M_{xy} \\ T_x \\ T_y \end{Bmatrix}=\mathbf{R}^0+\mathbf{R}^*+\mathbf{R}^f=\sum_{i=1}^{k}\mathbf{R}_i^0\beta_i+\mathbf{R}^*+\sum_{j=1}^{2}\mathbf{R}_j^f\alpha_j\ . \tag{22}$$

with

$$\mathbf{R}_j^f = \begin{Bmatrix} M_{xj}^f \\ M_{yj}^f \\ M_{xyj}^f \\ T_{xj}^f \\ T_{yj}^f \end{Bmatrix} = \begin{Bmatrix} -(1-\mu)D\dfrac{\partial^2 f_j}{\partial x \partial y} \\ (1-\mu)D\dfrac{\partial^2 f_j}{\partial x \partial y} \\ -\dfrac{1}{2}(1-\mu)D\left(\dfrac{\partial^2 f_j}{\partial y^2} - \dfrac{\partial^2 f_j}{\partial x^2}\right) \\ -C\dfrac{\partial f_j}{\partial y} \\ C\dfrac{\partial f_j}{\partial x} \end{Bmatrix}, \quad (j=1,2) \tag{23}$$

The detailed expressions of the resultants derived from f are given in Table II (Shang *et al.* 2015). It is shown that, these resultants are exponentially distributed along the direction perpendicular to the SS1 or FREE edge, while no exponential distributions exist along the direction parallel to the SS1 or FREE edge.

In order to formulate the elements HDF-P8-SS1(with SS1 edge effects) and HDF-P8-FREE(with free edge effects), the modified general solution part $\mathbf{S}_{\text{mod}}^{\text{edge}}$ and the modified particular solution part $\mathbf{R}_{\text{mod}}^{\text{edge}}$ when the plate is subjected to a uniformly distributed transverse load q are needed.

Element HDF-P8-SS1 or HDF-P8-FREE should be allocated along the SS1 or FREE edge of the plate (for example edge 12 in Figure 2). The boundary resultant force vector at the edge 12 should satisfy the following SS1 or FREE boundary conditions:

$$\bar{\mathbf{R}}_{\text{edge}} = \mathbf{L}_{\text{edge}}\mathbf{R}_{\text{edge}} = \mathbf{0}, \tag{24}$$

where

$$\begin{cases} \bar{\mathbf{R}}_{\text{SS1}} = \begin{Bmatrix} \bar{M}_n \\ \bar{M}_{ns} \end{Bmatrix}_{\text{SS1}} \\ \bar{\mathbf{R}}_{\text{FREE}} = \begin{Bmatrix} \bar{M}_n \\ \bar{M}_{ns} \\ \bar{T}_n \end{Bmatrix}_{\text{FREE}} \end{cases}, \tag{25}$$

$$\begin{cases} \mathbf{L}_{\mathrm{SS1}} = \begin{bmatrix} l_x^2 & l_y^2 & 2l_xl_y & 0 & 0 \\ -l_xl_y & l_xl_y & l_x^2-l_y^2 & 0 & 0 \end{bmatrix}_{\mathrm{SS1}} \\ \mathbf{L}_{\mathrm{FREE}} = \begin{bmatrix} l_x^2 & l_y^2 & 2l_xl_y & 0 & 0 \\ -l_xl_y & l_xl_y & l_x^2-l_y^2 & 0 & 0 \\ 0 & 0 & 0 & l_x & l_y \end{bmatrix}_{\mathrm{FREE}} \end{cases}, \tag{26}$$

$$\begin{cases} \mathbf{R}_{\mathrm{SS1}} = \mathbf{S}_{\Delta}^{\mathrm{SS1}}\boldsymbol{\beta}_{\Delta}^{\mathrm{SS1}} + \mathbf{S}_{\nabla}^{\mathrm{SS1}}\boldsymbol{\beta}_{\nabla}^{\mathrm{SS1}} + \mathbf{R}^{*} \\ \mathbf{R}_{\mathrm{FREE}} = \mathbf{S}_{\Delta}^{\mathrm{FREE}}\boldsymbol{\beta}_{\Delta}^{\mathrm{FREE}} + \mathbf{S}_{\nabla}^{\mathrm{FREE}}\boldsymbol{\beta}_{\nabla}^{\mathrm{FREE}} + \mathbf{R}^{*} \end{cases}, \tag{27}$$

in which:

$$\begin{cases} \mathbf{S}_{\Delta}^{\mathrm{SS1}} = \begin{bmatrix} \mathbf{R}_1^0 & \cdots & \mathbf{R}_{10}^0 & \mathbf{R}_{13}^0 & \mathbf{R}_{15}^0 & \mathbf{R}_{17}^0 & \cdots & \mathbf{R}_{23}^0 \end{bmatrix} \\ \mathbf{S}_{\Delta}^{\mathrm{FREE}} = \begin{bmatrix} \mathbf{R}_1^0 & \cdots & \mathbf{R}_5^0 & \mathbf{R}_7^0 & \mathbf{R}_8^0 & \mathbf{R}_9^0 & \mathbf{R}_{11}^0 & \mathbf{R}_{13}^0 & \mathbf{R}_{14}^0 & \mathbf{R}_{15}^0 & \mathbf{R}_{19}^0 & \mathbf{R}_{21}^0 & \mathbf{R}_{22}^0 & \mathbf{R}_{23}^0 \end{bmatrix} \end{cases}, \tag{28}$$

$$\begin{cases} \mathbf{S}_{\nabla}^{\mathrm{SS1}} = \begin{bmatrix} \mathbf{R}_{11}^0 & \mathbf{R}_{12}^0 & \mathbf{R}_{14}^0 & \mathbf{R}_{16}^0 & \mathbf{R}_1^f & \mathbf{R}_2^f \end{bmatrix} \\ \mathbf{S}_{\nabla}^{\mathrm{FREE}} = \begin{bmatrix} \mathbf{R}_6^0 & \mathbf{R}_{10}^0 & \mathbf{R}_{12}^0 & \mathbf{R}_{16}^0 & \mathbf{R}_{17}^0 & \mathbf{R}_{18}^0 & \mathbf{R}_{20}^0 & \mathbf{R}_1^f & \mathbf{R}_2^f \end{bmatrix} \end{cases}, \tag{29}$$

The detailed expressions of the matrices $\mathbf{S}_{\Delta}^{\mathrm{edge}}$ and $\mathbf{S}_{\nabla}^{\mathrm{edge}}$ can be obtained from Tables I and II. Substitution of Equations (28)-(29) into (27), then three sets of constraint equations can be obtained by substituting the coordinates (x_1, y_1), (x_2, y_2), (x_5, y_5) of nodes 1, 2, 5 into Equation (24):

$$\boldsymbol{\kappa}_{\Delta}^{\mathrm{edge}}\boldsymbol{\beta}_{\Delta}^{\mathrm{edge}} + \boldsymbol{\kappa}_{\nabla}^{\mathrm{edge}}\boldsymbol{\beta}_{\nabla}^{\mathrm{edge}} + \boldsymbol{\kappa}_{\Omega}^{\mathrm{edge}} = \mathbf{0}, \tag{30}$$

with

$$\begin{cases} \boldsymbol{\kappa}_{\Delta}^{\mathrm{SS1}} = \begin{bmatrix} \mathbf{L}_{\mathrm{SS1}}\mathbf{S}_{\Delta}^{\mathrm{SS1}}(x_1,y_1) \\ \mathbf{L}_{\mathrm{SS1}}\mathbf{S}_{\Delta}^{\mathrm{SS1}}(x_2,y_2) \\ \mathbf{L}_{\mathrm{SS1}}\mathbf{S}_{\Delta}^{\mathrm{SS1}}(x_5,y_5) \end{bmatrix}, \boldsymbol{\kappa}_{\nabla}^{\mathrm{SS1}} = \begin{bmatrix} \mathbf{L}_{\mathrm{SS1}}\mathbf{S}_{\nabla}^{\mathrm{SS1}}(x_1,y_1) \\ \mathbf{L}_{\mathrm{SS1}}\mathbf{S}_{\nabla}^{\mathrm{SS1}}(x_2,y_2) \\ \mathbf{L}_{\mathrm{SS1}}\mathbf{S}_{\nabla}^{\mathrm{SS1}}(x_5,y_5) \end{bmatrix}, \boldsymbol{\kappa}_{\Omega}^{\mathrm{SS1}} = \begin{bmatrix} \mathbf{L}_{\mathrm{SS1}}\mathbf{R}^{*}(x_1,y_1) \\ \mathbf{L}_{\mathrm{SS1}}\mathbf{R}^{*}(x_2,y_2) \\ \mathbf{L}_{\mathrm{SS1}}\mathbf{R}^{*}(x_5,y_5) \end{bmatrix} \\ \boldsymbol{\kappa}_{\Delta}^{\mathrm{FREE}} = \begin{bmatrix} \mathbf{L}_{\mathrm{FREE}}\mathbf{S}_{\Delta}^{\mathrm{FREE}}(x_1,y_1) \\ \mathbf{L}_{\mathrm{FREE}}\mathbf{S}_{\Delta}^{\mathrm{FREE}}(x_2,y_2) \\ \mathbf{L}_{\mathrm{FREE}}\mathbf{S}_{\Delta}^{\mathrm{FREE}}(x_5,y_5) \end{bmatrix}, \boldsymbol{\kappa}_{\nabla}^{\mathrm{FREE}} = \begin{bmatrix} \mathbf{L}_{\mathrm{FREE}}\mathbf{S}_{\nabla}^{\mathrm{FREE}}(x_1,y_1) \\ \mathbf{L}_{\mathrm{FREE}}\mathbf{S}_{\nabla}^{\mathrm{FREE}}(x_2,y_2) \\ \mathbf{L}_{\mathrm{FREE}}\mathbf{S}_{\nabla}^{\mathrm{FREE}}(x_5,y_5) \end{bmatrix}, \boldsymbol{\kappa}_{\Omega}^{\mathrm{FREE}} = \begin{bmatrix} \mathbf{L}_{\mathrm{FREE}}\mathbf{R}^{*}(x_1,y_1) \\ \mathbf{L}_{\mathrm{FREE}}\mathbf{R}^{*}(x_2,y_2) \\ \mathbf{L}_{\mathrm{FREE}}\mathbf{R}^{*}(x_5,y_5) \end{bmatrix} \end{cases}, \tag{31}$$

where $\boldsymbol{\kappa}_{\Delta}^{\mathrm{SS1}}$ is a 6×19 matrix; $\boldsymbol{\kappa}_{\nabla}^{\mathrm{SS1}}$ is a 6×6 matrix; $\boldsymbol{\kappa}_{\Omega}^{\mathrm{SS1}}$ is a 6×1 matrix; $\boldsymbol{\kappa}_{\Delta}^{\mathrm{FREE}}$ is a 9×17 matrix; $\boldsymbol{\kappa}_{\nabla}^{\mathrm{FREE}}$ is a 9×9 matrix; and $\boldsymbol{\kappa}_{\Omega}^{\mathrm{FREE}}$ is a 9×1 matrix. Then, the vector $\boldsymbol{\beta}_{\nabla}^{\mathrm{edge}}$ can be solved by:

$$\boldsymbol{\beta}_{\nabla}^{\mathrm{edge}} = -\boldsymbol{\kappa}_{\nabla}^{\mathrm{edge}^{-1}}(\boldsymbol{\kappa}_{\Delta}^{\mathrm{edge}}\boldsymbol{\beta}_{\Delta}^{\mathrm{edge}} + \boldsymbol{\kappa}_{\Omega}^{\mathrm{edge}}), \tag{32}$$

Substitution of Equation (32) into (27) yields

$$\mathbf{R}_{\mathrm{edge}} = \mathbf{S}_{\mathrm{mod}}^{\mathrm{edge}}\boldsymbol{\beta}_{\Delta}^{\mathrm{edge}} + \mathbf{R}_{\mathrm{mod}}^{\mathrm{edge}}, \tag{33}$$

where

$$\mathbf{S}_{\text{mod}}^{\text{edge}} = \mathbf{S}_{\Delta}^{\text{edge}} - \mathbf{S}_{\nabla}^{\text{edge}} \boldsymbol{\kappa}_{\nabla}^{\text{edge}^{-1}} \boldsymbol{\kappa}_{\Delta}^{\text{edge}}, \tag{34}$$

$$\mathbf{R}_{\text{mod}}^{\text{edge}} = \mathbf{R}^{*} - \mathbf{S}_{\nabla}^{\text{edge}} \boldsymbol{\kappa}_{\nabla}^{\text{edge}^{-1}} \boldsymbol{\kappa}_{\Omega}^{\text{edge}}. \tag{35}$$

Equation (34) is the final modified trial functions for resultants of element HDF-P8-SS1 or HDF-P8-FREE, which can satisfy the boundary conditions at the nodes along the SS1 or FREE edge. $\mathbf{S}_{\text{mod}}^{\text{edge}}$ is the modified general solution part; $\boldsymbol{\beta}_{\Delta}^{\text{edge}}$ is the final unknown coefficient vector; $\mathbf{R}_{\text{mod}}^{\text{edge}}$ is the modified particular solution part when the plate is subjected to a uniformly distributed transverse load q.

In order to derive the formulations of the element HDF-P8-SS1 and the element HDF-P8-FREE, the $\hat{\mathbf{S}}$ and $\mathbf{R}^{*}$ from Equations (9) to (12) can be simply substituted by $\mathbf{S}_{\text{mod}}^{\text{edge}}$, $\mathbf{R}_{\text{mod}}^{\text{edge}}$ respectively. The other procedures are the same as the formulations of element HDF-P8-23β.

4. Numerical examples

In this section, the performances of the proposed elements HDF-P8-23β, HDF-P8-SS1 and HDF-P8-FREE are fully assessed by some classic benchmark examples. Both traditional and new severely distorted meshes are employed. Meanwhile, the results calculated by element S8R in *Abaqus* (2009), some other well-known high-order quadrilateral elements, and the low-order hybrid displacement function elements proposed by Cen *et al*. (2014), Shang *et al.* (2015) are also given for comparison.

4.1. Eigenvalues and rank

It is found that, for extremely thin and moderately thick plate cases, each element stiffness matrix of three new elements always produces only three zero eigenvalues corresponding to three rigid body modes for various regular or distorted element shapes. As a result, the proper rank and the absence of spurious modes can ensure that proposed elements are stable.

4.2. Patch tests for element HDF-P8-23β

Figure 3 plots the Irons patch test problems. These tests are only performed for element HDF-P8-23β without edge effect. And different test conditions are summarized as follows:

i) Meshes: Four mesh types are employed. Mesh A contains only one 8-node element, while Meshes B, C and D are divided into five distorted elements.

ii) Loads and Constraints: Distributed line loads along the patch boundaries; three nodal deflections are constrained (w_1=w_2=w_3=0) to eliminate rigid body motions.

iii) Span-thickness ratios: Three different span-thickness ratios 2a/h=1000, 100, 10, are considered.

(a) *Constant bending moment case* (M_n= 1). As shown in Figure 3a, the rectangular plate patch is subjected to bending moment M_n= 1 along its all edges. The computed results of bending moments M_x (=1) and M_y (=1), twisting moment M_{xy} (=0), shear forces T_x (=0) and T_y (=0), at any point are exact for all span-thickness ratio cases.

(b) *Constant twisting moment case* (M_{ns}= 1). As shown in Figure 3b, the rectangular plate patch is subjected to twisting moment M_{ns}= 1 along its four edges. In all cases, the numerical results of M_{xy} (=1), M_x (=0), M_y (=0) T_x (=0) and T_y (=0) obtained by the element HDF-P8-23β are exact.

(c) *Non-zero constant shear force case* (T_x=Constant, T_y=Constant). As shown in Figure 3c, the eight boundary nodes of the rectangular plate patch are imposed by given deflections and rotations. The element HDF-P8-23β can give the exact constant shear force (T_x=Constant, T_y=Constant) corresponding to different span-thickness ratio cases.

4.3. Square plate subjected to uniformly distributed load

Figure 4 gives the meshes employed for this example, in which only a quarter of the plate is considered owing to the biaxial symmetry. The geometric parameters and conditions are given as follows:

i) Geometric parameters: L denotes the edge length; h denotes the thickness of the plate; Poisson's ratio μ= 0.3.

ii) Load and Boundary Conditions (BCs): The square plate is subjected to a uniform transverse load q=1. Three BC cases, the clamped BC (w=0, ψ_n=0, ψ_s=0), the soft simply supported (SS1) BC (w=0), and the hard simply supported (SS2) BC (w=0, ψ_s=0), are considered.

iii) Span-thickness ratios: From thick case (h/L=0.1) to very thin case (h/L=10^{-30})

iv) Meshes: Three mesh types are used, and the mesh densities are 1×1, 2×2, 4×4, 8×8 and 16×16.

The dimensionless results (here, let L =1 and D =1) of deflections and moments at the plate center are presented in Tables III to V. It should be noted that under SS1 BC, edge effect will take place. So, as shown in Figure 4, element HDF-P8-SS1 will be allocated along the SS1 boundary, in which the corner region is split into two degenerated triangular elements. Since the shapes of the present elements are quite free, such mesh will not bring unfavorable influence. The corresponding results are given in Tables III to V, and plotted in Figures 5 to 7. From Figures 5(c), 6(c) and 7(c), the distributions of the bending moments and the shear forces under different boundary conditions are clearly visualized. And the influence of the edge effects for shear force T_x can be observed in Figure 7(c). The new elements exhibit excellent performance for both precision and convergence for this example.

4.4. Test for checking the sensitivity problem to mesh distortions

As shown in Figure 8, several distorted meshes are designed to test the sensitivity to mesh distortions for the new element HDF-P8-23β. A quarter of thin square plate with symmetry and clamped boundary conditions is subjected to a uniformly distributed load. All parameters are the same as those given in section 4.3.

The normalized results of the central deflection and moment of the plate are also given in Figure 8. It can be seen that element HDF-P8-23β is quite roust even when the mesh is severely distorted.

4.5. Skew plates subjected to uniformly distributed load

Figure 9 shows a new 4×4 mesh configuration and the geometric parameters for a 30° skew plate with SS1 BC (soft simply supported). This example has been studied by Morley (1963) under the thin plate assumptions. Two characters exists in this test: i) singularity appears in the bending moment at the obtuse corner; and ii) edge effect appears. This problem has also been solved as a 3D elastic case by Babuška and Scapolla (1989). Two span-thickness ratios (L/h=1000, 100) are considered. The principal bending moments and deflections at the central node O are

calculated. Table VI, Table VII and Figure 10 present the dimensionless results obtained by the new elements HDF-P8-23β and HDF-P8-SS1 (due to the occurrence of the edge effects) and other models. Better convergence can be obtained by the new models when compared to other elements.

4.6. Circular plate subjected to uniformly distributed load

Figure 11 shows a circular plate subjected to a uniform load q = 1. According to the symmetry, only a quarter of the plate is modeled. Two different thickness-radius ratio cases (h/R=0.02, 0.2), and two different BC cases, the soft simply supported (SSl) BC (w = 0) and the clamped BC (w=0, ψ_n=0, ψ_s=0), are considered. The analytical solutions can be found in references (Ayad *et al*. 1998; Ayad and Rigolot 2002). Results obtained by the new element HDF-P8-23β and some other models are given in Tables VIII, IX and plotted in Figure 12, 13.

Because HDF-P8-23β is a high-order element with mid-side nodes, it is possible for the element to simulate the circular arc. This example can be perfectly solved by only using one HDF-P8-23β element, which cannot be achieved by other models in different literatures. Although the test contains the SS1 boundary condition, according to the Mindlin-Reissner theory, the edge effects will not take place in the circular plate case. So, satisfactory solutions can be obtained by using element HDF-P8-23β only.

4.7. Edge effect test

As shown in Figure 14, a square plate is subjected to a uniformly transverse load q. Due to symmetry, only one quarter of the plate, ABCD (C is the center of the plate), is analyzed. Two boundary condition cases are studied: (i) *SFSF*, two opposite edges hard simply-supported (SS2) and the other two edges free; and (ii) SS^*SS^*, two opposite edges hard simply-supported (SS2) and the other two edges soft simply-supported (SS1). The edge length of the square plate is a, the thickness is h, and Poisson's ratio μ = 0.3. And only one span-thickness ratio, a/h=50, is considered.

Kant and Hinton (1983,2002) have solved the case by using the segmentation method. Thus, their solutions are presented here for comparison. Furthermore, results obtained by some other 4-, 5- and 8-node quadrilateral plate elements, including Shang *et al.* (2015), S4 (*Abaqus* 2009), S8R (*Abaqus* 2009), HMPL5 (Saleeb and Chang 1987) and CL8 (Spilker 1982), are also presented for

comparison.

a) The SFSF plate

The meshes and the locations of the elements HDF-P8-Free and HDF-P8-23β are also illustrated in Figure 14. The values of displacements and resultants at selected points, obtained by present method and Shang *et al* (2015), Abaqus elements S8R (*Abaqus* 2009), are listed in Table X for comparing the convergence rate. And the results derived by two semi-analytic methods, including the segmentation method (Kant and Gadgil 2002; Kant and Hinton 1983) and the FEMOL (Yuan 1993), are also presented.

The distributions of the resultants obtained by the present scheme along selected paths and the corresponding contour plots of the resultants are plotted through Figures 15 to 16. The values at nodes are smoothed solutions by averaging direct nodal values at all connective elements.

Figure 15 plots the distribution of T_x along the symmetry edge DC. Figure 16 shows the distributions of M_{xy} and T_y along the hard simply-supported edge AB. Their distributions recalculated by the present method using a 10×10 mesh, and results of some other quadrilateral plate elements are also given for comparison.

From the numerical results, some conclusions could be drawn:

i) Compared to other elements, the combination of HDF-P8-Free and HDF-P8-23β exhibits better prediction and convergence for the resultants. Meanwhile, for present elements, only a coarse mesh is enough to ensure that the zero resultant conditions are satisfied at the nodes along free edge.

ii) Compared to the low-order element proposed by Shang *et al.* (2015), the present element combination shows better performance in capturing the peak value of the resultants.

b) The SS*SS* case

The meshes and the location of the elements HDF-P8-SS1 and HDF-P8-23β are also illustrated in Figure 14. And for the case a/h=50, the results calculated at selected points are listed in Table XI. Figure 17 shows the distribution of T_x along the symmetry edge DC. Figure 18 shows the distributions of M_{xy} and T_y along the hard simply-supported edge AB. The corresponding contour plots of the resultant are also presented. Results calculated by some other quadrilateral plate elements with a 10×10 mesh are also given for comparison. Same conclusions

as those in previous case can be obtained.

5. Conclusions

In this paper, three simple high-order hybrid displacement function elements are presented for analysis of thin and moderately thick plates. In general situation, the displacement function F, which can be used to derive displacement components satisfying all governing equations, is combined with the locking-free arbitrary order Timoshenko's beam functions. Then, an 8-node, 24-DOF quadrilateral plate bending element, HDF-P8-23β, is formulated. For the special situation consisting of the edge effect or the boundary layer effect (SS1 or FREE type), an additional displacement function f related to the edge effect is considered to develop novel plate bending elements HDF-P8-SS1 or HDF-P8-FREE.

Numerical examples show that the proposed elements are free of shear-locking, pass all patch tests, exhibit excellent convergence, and possess higher precision when compared to other existing models, even when quite coarse and extremely distorted meshes are used. Especially, they can effectively solve the edge effect by accurately capturing the peak value and the sharp changes of stress/resultant-force near the SS1 or Free boundary.

The proposed method possesses advantages from both analytical and discrete methods, and can be easily integrated into the standard framework of finite element programs. An interesting future work is to develop a high performance plate crack element, and then combine the proposed elements with plate crack element to solve the plate crack propagation problem of the plate.

Appendix: The expressions for matrix $\bar{\mathbf{N}}\big|_\Gamma$ in Equation (12)

The *i-j-k* boundary displacement vector of the element $\bar{\mathbf{N}}\big|_\Gamma$ can be rewritten as

$$\bar{\mathbf{d}} = \begin{Bmatrix} \bar{\psi}_n \\ \bar{\psi}_s \\ \bar{w} \end{Bmatrix} = \mathbf{L}_d \bar{\mathbf{u}}_{ijk} = \bar{\mathbf{N}}\big|_\Gamma \mathbf{q}^e , \tag{A1}$$

in which the vector $\bar{\mathbf{u}}_{ijk}$ is given by Equation (6); and $\mathbf{L}_d$ is the direction matrix,

$$\mathbf{L}_d = \begin{bmatrix} 0 & l_x & l_y \\ 0 & -l_y & l_x \\ 1 & 0 & 0 \end{bmatrix}. \tag{A2}$$

- Along 1-2-5 boundary,

$$\bar{\mathbf{N}}\big|_\Gamma = \begin{bmatrix} \mathbf{N}_1 & \mathbf{N}_2 & \mathbf{0} & \mathbf{0} & \mathbf{N}_5 & \mathbf{0} & \mathbf{0} & \mathbf{0} \end{bmatrix}, \tag{A3}$$

where

$$\mathbf{N}_1 = \begin{bmatrix} 0 & I_a l_x & I_a l_y \\ 0 & -I_a l_y & I_a l_x \\ I_a & -I_0 l_x^* & I_0 l_y^* \end{bmatrix}, \mathbf{N}_2 = \begin{bmatrix} 0 & I_b l_x & I_b l_y \\ 0 & -I_b l_y & I_b l_x \\ I_b & -I_0 l_x^* & I_0 l_y^* \end{bmatrix}, \mathbf{N}_5 = \begin{bmatrix} 0 & I_c l_x & I_c l_y \\ 0 & -I_c l_y & I_c l_x \\ I_c & 2I_0 l_x^* & -2I_0 l_y^* \end{bmatrix}, \tag{A4}$$

and $\mathbf{0}$ is a 3×3 zero matrix.

- Along 2-3-6 boundary,

$$\bar{\mathbf{N}}\big|_\Gamma = \begin{bmatrix} \mathbf{0} & \mathbf{N}_2 & \mathbf{N}_3 & \mathbf{0} & \mathbf{0} & \mathbf{N}_6 & \mathbf{0} & \mathbf{0} \end{bmatrix}, \tag{A5}$$

where

$$\mathbf{N}_2 = \begin{bmatrix} 0 & I_a l_x & I_a l_y \\ 0 & -I_a l_y & I_a l_x \\ I_a & -I_0 l_x^* & I_0 l_y^* \end{bmatrix}, \mathbf{N}_3 = \begin{bmatrix} 0 & I_b l_x & I_b l_y \\ 0 & -I_b l_y & I_b l_x \\ I_b & -I_0 l_x^* & I_0 l_y^* \end{bmatrix}, \mathbf{N}_6 = \begin{bmatrix} 0 & I_c l_x & I_c l_y \\ 0 & -I_c l_y & I_c l_x \\ I_c & 2I_0 l_x^* & -2I_0 l_y^* \end{bmatrix}. \tag{A6}$$

- Along 3-4-7 boundary,

$$\bar{\mathbf{N}}\big|_\Gamma = \begin{bmatrix} \mathbf{0} & \mathbf{0} & \mathbf{N}_3 & \mathbf{N}_4 & \mathbf{0} & \mathbf{0} & \mathbf{N}_7 & \mathbf{0} \end{bmatrix}, \tag{A7}$$

where

$$\mathbf{N}_3 = \begin{bmatrix} 0 & I_a l_x & I_a l_y \\ 0 & -I_a l_y & I_a l_x \\ I_a & -I_0 l_x^* & I_0 l_y^* \end{bmatrix}, \mathbf{N}_4 = \begin{bmatrix} 0 & I_b l_x & I_b l_y \\ 0 & -I_b l_y & I_b l_x \\ I_b & -I_0 l_x^* & I_0 l_y^* \end{bmatrix}, \mathbf{N}_7 = \begin{bmatrix} 0 & I_c l_x & I_c l_y \\ 0 & -I_c l_y & I_c l_x \\ I_c & 2I_0 l_x^* & -2I_0 l_y^* \end{bmatrix}, \tag{A8}$$

- Along 4-1-8 boundary,

$$\bar{\mathbf{N}}\big|_\Gamma = \begin{bmatrix} \mathbf{N}_1 & \mathbf{0} & \mathbf{0} & \mathbf{N}_4 & \mathbf{0} & \mathbf{0} & \mathbf{0} & \mathbf{N}_8 \end{bmatrix}, \tag{A9}$$

where

$$\mathbf{N}_4 = \begin{bmatrix} 0 & I_a l_x & I_a l_y \\ 0 & -I_a l_y & I_a l_x \\ I_a & -I_0 l_x^* & I_0 l_y^* \end{bmatrix}, \mathbf{N}_1 = \begin{bmatrix} 0 & I_b l_x & I_b l_y \\ 0 & -I_b l_y & I_b l_x \\ I_b & -I_0 l_x^* & I_0 l_y^* \end{bmatrix}, \mathbf{N}_8 = \begin{bmatrix} 0 & I_c l_x & I_c l_y \\ 0 & -I_c l_y & I_c l_x \\ I_c & 2I_0 l_x^* & -2I_0 l_y^* \end{bmatrix}. \tag{A10}$$

The relevant parameters and matrices have been given in Equations (3) to (7).

References

Abaqus 6.9 (2009) HTML Documentation. Dassault Systèmes Simulia Corp.: Providence, RI, USA.

Ahmad, S., Irons, M. and Zienkiewicz, O. C., (1970) "Analysis of thick and thin shell structures by curved finite elements", International Journal for Numerical Methods in Engineering, Vol.2, pp. 419-451.

Arnold, D.N. and Falk, R.S., (1989) "Edge effects in the Reissner-Mindlin plate theory". Analytical and Computational Models for Shells, pp. 71-90.

Arnold, D.N. and Falk, R.S., (1990) "The boundary layer for the Reissner-Mindlin plate model", SIAM Journal on Mathematical Analysis, Vol.21 No.2, pp. 281-312.

Ayad, R., Dhatt, G. and Batoz, J. L., (1998) "A new hybrid-mixed variational approach for Reissner-Mindlin plates. The MiSP Model", *International Journal for Numerical Methods in Engineering*, Vol.42, pp. 1149-1179.

Ayad, R. and Rigolot, A., (2002) "An improved four-node hybrid-mixed element based upon Mindlin's plate theory", *International Journal for Numerical Methods in Engineering*, Vol.55, pp. 705-731.

Babuška, I. and Scapolla, T., (1989) "Benchmark computation and performance evaluation for a rhombic plate bending problem", *International Journal for Numerical Methods in Engineering*, Vol.28 No.1, pp. 155-179.

Bathe, K. J. (1996), *Finite Element Procedures*. Prentice Hall: New Jersey.

Bathe, K. J. and Dvorkin, E. N., (1985) "A four-node plate bending element based on Mindlin–Reissner plate theory and a mixed interpolation", *International Journal for Numerical Methods in Engineering*, Vol.21 No.2, pp. 367-383.

Bathe, K. J. and Dvorkin, E. N., (1986) "A formulation of general shell elements—the use of mixed interpolation of tensorial components", *International Journal for Numerical Methods in Engineering*, Vol.22 No.3, pp. 697-722.

Batoz, J. L. and Lardeur, P., (1989) "A discrete shear triangular nine dof element for the analysis of thick to very thin plate", *International Journal for Numerical Methods in Engineering*, Vol.28, pp. 533-560.

Belytschko, T. and Tsay, C.S., (1983) "A stabilization procedure for the quadrilateral plate element with one point quadrature", *International Journal for Numerical Methods in Engineering*, Vol.19 No.3, pp. 405-419.

Belytschko, T., Tsay, C. S. and Liu, W. K., (1981) "A stabilization matrix for the bilinear Mindlin plate element", *Computer Methods in Applied Mechanics and Engineering*, Vol.29 No.3, pp. 313-327.

Briassoulis, D., (1993a) "Modeling edge effects with the C0 plate-bending elements: Part 1. Analysis of the mechanism", *International Journal for Numerical Methods in Engineering*, Vol.36 No.23, pp. 4045-4068.

Briassoulis, D., (1993b) "Modeling edge effects with the C0 plate-bending elements: Part 2. The performance of the reformulated four-node element", *International Journal for Numerical Methods in Engineering*, Vol.36 No.23, pp. 4069-4109.

Cen, S., Fu, X.-R. and Zhou, M.-J. (2011a), "8-and 12-node plane hybrid stress-function elements immune to severely distorted mesh containing elements with concave shapes", *Computer Methods in Applied Mechanics and Engineering*, Vol.200 No.29, pp. 2321-2336..

Cen, S., Fu, X. R., Zhou, G. H., Zhou, M. J. and Li, C. F., (2011b) "Shape-free finite element method: The plane Hybrid Stress-Function (HS-F) element method for anisotropic materials", *SCIENCE CHINA Physics, Mechanics & Astronomy*, Vol.54 No.4, pp. 653-665.

Cen, S., Long, Y. Q. and Yao, Z. H., (2002) "A new hybrid-enhanced displacement-based element for the analysis of laminated composite plates", *Computers & Structures*, Vol.80 No.9-10, pp. 819-833.

Cen, S., Long, Y. Q., Yao, Z. H. and Chiew, S. P., (2006) "Application of the quadrilateral area co-ordinate method: A new element for Mindlin-Reissner plate", *International Journal for*

Numerical Methods in Engineering, Vol.66 No.1, pp. 1-45.

Cen, S., Shang, Y., Li, C. -F. and Li, H. -G. (2014), "Hybrid displacement function element method: a simple hybrid-Trefftz stress element method for analysis of Mindlin-Reissner plate", *International Journal for Numerical Methods in Engineering*, Vol.98 No.3, pp. 203-234.

Cen, S., and Shang, Y. (2015), "Developments of Mindlin-Reissner Plate Elements", *Mathematical Problems in Engineering*, Vol. 2015, ID 456740.

Cen, S., and Shang, Y. (2015), "Developments of Mindlin-Reissner Plate Elements", *Mathematical Problems in Engineering*, Vol. 2015, ID 456740.

Cen, S., Zhou, M. J. and Fu, X. R., (2011c) "A 4-node hybrid stress-function (HS-F) plane element with drilling degrees of freedom less sensitive to severe mesh distortions", *Computers & Structures*, Vol.89 No.5-6, pp. 517-528.

Chen, W. J. and Cheung, Y. K., (2000) "Refined quadrilateral element based on Mindlin/Reissner plate theory", *International Journal for Numerical Methods in Engineering*, Vol.47, pp. 605-627.

Crisfield, M. A., (1984), "A quadratic Mindlin element using shear constraints", *Computers & Structures*, Vol.18 No.5, pp. 833-852.

Dhananjaya, H. R., Pandey, P. C. and Nagabhushanam, J., (2009) "New eight node serendipity quadrilateral plate bending element for thin and moderately thick plates using integrated force method", *Structural Engineering and Mechanics*, Vol.33 No.4, pp. 485-508.

Donea, J. and Lamain, L.G., (1987) "A modified representation of transverse shear in C0 quadrilateral plate elements", *Computer Methods in Applied Mechanics and Engineering*, Vol.63, pp. 183-207.

Falsone, G. and Settineri, D., (2012) "A Kirchhoff-like solution for the Mindlin plate model: A new finite element approach", *Mechanics Research Communications*, Vol.40, pp. 1-10.

Fu, X. R., Cen, S., Li, C. F. and Chen, X. M., (2010) "Analytical trial function method for development of new 8-node plane element based on the variational principle containing Airy stress function", *Engineering Computations*, Vol.27 No.4, pp. 442-463.

Haggblad, B. and Bathe, K. J., (1990) "Specifications of boundary-conditions for Reissner-Mindlin plate bending finite-elements", *International Journal for Numerical Methods in Engineering*, Vol.30 No.5, pp. 981-1011.

Hansbo, P., Heintz, D. and Larson, M.G., (2011) "A finite element method with discontinuous rotations for the Mindlin-Reissner plate model", *Computer Methods in Applied Mechanics and Engineering*, Vol. 200 No.5-8, pp. 638-648.

Hinton, E. and Huang, H. C., (1986) "A family of quadrilateral Mindlin plate element with substitute shear strain fields", *Computers & Structures*, Vol.23 No.3, pp. 409-431.

Hinton, E., Selman, A., Alkhamis, M., (1995) "Boundary-layers in uniform and variable thickness plates with rectangular and curved planforms using the finite strip method", *Communications in Numerical Methods in Engineering*, Vol.11 No.7, pp. 597-606.

Hu, B., Wang, Z. and Xu, Y. C., (2010) "Combined hybrid method applied in the Reissner–Mindlin plate model", *Finite Elements in Analysis and Design*, Vol.46, pp. 428–437.

Hughes, T. J. R. and Cohen, M., (1978) "The "heterosis" finite element for plate bending", *Computers & Structures*, Vol:9, pp. 445-450.

Hughes, T. J. R., Taylor, R. L., and Kanoknukulchai, W., (1977) "A simple and efficient finite element for plate bending", *International Journal for Numerical Methods in Engineering*, Vol.11 No.10, pp. 1529-1543.

Hu, H.C., (1984) *Variational principle of Theory of Elasticity with Applications*.Science press, Gordon and Breach, Science publisher: Beijing.

Ibrahimbegović, A., (1993) "Quadrilateral finite elements for analysis of thick and thin plates", *Computer Methods in Applied Mechanics and Engineering*, Vol.110, pp. 195-209.

Jelenic, G. and Papa, E., (2011) "Exact solution of 3D Timoshenko beam problem using linked interpolation of arbitrary order", *Archive of Applied Mechanics*, Vol.18, pp. 171-183.

Jin, F.S. and Qin, Q. H., (1995) "A variational principle and hybrid Trefftz finite-element for the analysis of Reissner plates", *Computers & Structures*, Vol.56 No.4, pp. 697-701.

Jin, W. G., Cheung, Y. K. and Zienkiewicz, O. C., (1993) "Trefftz method for Kirchhoff plate bending problems", *International Journal for Numerical Methods in Engineering*, Vol.36, pp. 765-781.

Jirousek, J., Wróblewski, A., Qin, Q. H. and He, X. Q., (1995a) "A family of quadrilateral hybrid-Trefftz p-elements for thick plate analysis", *Computer Methods in Applied Mechanics and Engineering*, Vol.127, pp. 315-344.

Jirousek, J., Wróblewski, A. and Szybinski, B., (1995b) "A new 12 DOF quadrilateral element for analysis of thick and thin plates", *International Journal for Numerical Methods in Engineering*, Vol:38, pp. 2619-2638.

Kant, T. and Gadgil, M. G., (2002) "Analysis of orthotropic plates based on three theories by segmentation method", *Mechanics of Advanced Materials and Structures*, Vol.9 No.3, pp. 189-239.

Kant, T. and Hinton, E., (1983) "Mindlin plate analysis by segmentation method"., *Journal of Engineering Mechanics-ASCE*, Vol.109 No.2, pp. 537-556.

Kant, T., Owen, D.R.J. and Zienkiewicz, O.C., (1982) "A refined higher-order C0 plate bending element", *Computers & Structures*, Vol.15 No.2, pp. 177-183.

Katili, I., (1993) "A new discrete Kirchhoff-Mindlin element based on Mindlin-Reissner plate theory and assumed shear strain fields—Part II: An extended DKQ element for thick-plate bending analysis", *International Journal for Numerical Methods in Engineering*, Vol.36 No.11, pp. 1885-1908.

Lee, S.W. and Wong, S. C., (1982) "Mixed formulation finite elements for Mindlin theory plate bending", *International Journal for Numerical Methods in Engineering*, Vol.18 No.9, pp. 1297-1311.

Li, T., Qi, Z. H., Ma, X. and Chen, W. J., (2015) "High-order assumed stress quadrilateral element for the Mindlin plate bending problem", *Structural Engineering and Mechanics*, Vol.54 No.3, pp. 393-417.

Long, Y.-Q., Cen, S. and Long, Z.-F. (2009), *Advanced finite element method in structural engineering*, Springer, Heidelberg & Tsinghua University Press, Beijing.

Long, Y. Q., Li, J. X., Long, Z. F. and Cen, S., (1999) "Area coordinates used in quadrilateral elements", *Communications in Numerical Methods in Engineering*, Vol.15 No.8, pp. 533-545.

Long, Z. F., Li, J. X., Cen, S. and Long, Y. Q., (1999) "Some basic formulae for area coordinates used in quadrilateral elements", *Communications in Numerical Methods in Engineering*, Vol.15 No.12, pp. 841-852.

Mindlin, R. D. (1951), "Influence of rotatory inertia and shear on flexural motions of isotropic elastic plates", *Journal of Applied Mechanics-Transactions of the Asme*, Vol. 18 No.1, pp. 31-38.

Morley, L.S.D., (1963) *Skew Plates and Structures*. International Series of Monographs in Aeronautics and Astronautics. Macmillan: New York.

Nguyen-Thanh, N., Rabczuk, T., Nguyen-Xuan, H. and Bordas, S., (2011) "An alternative alpha finite element method with discrete shear gap technique for analysis of isotropic Mindlin-Reissner plates", *Finite Elements in Analysis and Design*, Vol.47 No.5, pp. 519-535.

Nguyen-Thoi, T., Phung-Van, P., Nguyen-Xuan, H. and Thai-Hoang, C., (2012) "A cell-based smoothed discrete shear gap method using triangular elements for static and free vibration analyses of Reissner-Mindlin plates", *International Journal for Numerical Methods in Engineering*, Vol.91 No.7, pp. 705-741.

Nguyen-Xuan, H., Liu, G. R., Thai-Hoang, C. and Nguyen-Thoi, T., (2009) "An edge-based smoothed finite element method with stabilized discrete shear gap technique for analysis of Reissner–Mindlin plates", *Computer Methods in Applied Mechanics and Engineering*, Vol.199, pp. 471–489.

Nguyen-Xuan, H., Rabczuk, T., Bordas, S. and Debongnie, J. F. (2008), "A smoothed finite element method for plate analysis", *Computer Methods in Applied Mechanics and Engineering*, Vol.197 No.13-16, pp. 1184-1203.

Onate, E., Zienkiewicz, O. C., Suarez, B. and Taylor, R. L., (1992) "A general methodology for deriving shear constrained Reissner–Mindlin plate elements", *International Journal for Numerical Methods in Engineering*, Vol.33 No.2, pp. 345-367.

Petrolito, J., (1990) "Hybrid-Trefftz quadrilateral elements for thick plate analysis", *Computer Methods in Applied Mechanics and Engineering*, Vol.78 No.3, pp. 331-351.

Petrolito, J., (1996) "Triangular thick plate elements based on a hybrid-Trefftz approach", *Computers & Structures*, Vol.60 No.6, pp. 883-894.

Polit, O., Touratier, M. and Lory, P., (1994) "A new eight-node quadrilateral shear-bending plate finite element", *International Journal for Numerical Methods in Engineering*, Vol.37, pp. 387-411.

Rao, N.V. R., Ozakca, M. and Hinton, E., (1992) "A study of boundary-layers in plates using Mindlin-Reissner and 3-D elements", *International Journal for Numerical Methods in Engineering*, Vol.33 No.6, pp. 1305-1320.

Reissner, E. (1945), "The effect of transverse shear deformation on the bending of elastic plates", *Journal of Applied Mechanics-Transactions of the Asme*, Vol. 12 No.2, pp. 69-77.

Rezaiee-Pajand, M. and Karkon, M., (2012) "Two efficient hybrid-Trefftz elements for plate bending analysis", *Latin American Journal of Solids and Structures*, Vol.9 No.1, pp. 43-67.

Ribaric, D. and Jelenic, G., (2012) "Higher-order linked interpolation in quadrilateral thick plate finite elements", *Finite Elements in Analysis and Design*, Vol.51, pp. 67-80.

Saleeb, A. F. and Chang, T. Y., (1987) "An efficient quadrilateral element for plate bending analysis", *International Journal for Numerical Methods in Engineering*, Vol.24, No.6, pp. 1123-1155.

Schwab, C. and Suri, M., (1996) "The *p* and *hp* versions of the finite element method for problems with boundary layers", *Mathematics of Computation*, Vol.65 No.216, pp. 1403-1429.

Shang, Y., Cen, S., Li, C.-F. and Huang, J.-B. (2015a), "An effective hybrid displacement function element method for solving the edge effect of Mindlin-Reissner plate", *International Journal for Numerical Methods in Engineering*, Vol. 102, pp. 1449-1487.

Soh, A. -K., Cen, S., Long, Y. -Q. and Long, Z. -F. (2001), "A new twelve DOF quadrilateral element for analysis of thick and thin plates", *European Journal of Mechanics A-Solids*, Vol.20 No.2, pp. 299-326.

Soh, A. -K., Long, Z. -F. and Cen, S., (1999a) "A Mindlin plate triangular element with improved interpolation based on Timoshenko's beam theory", *Communications in Numerical Methods in Engineering*, Vol.15 No.7, pp. 527-532.

Soh, A. -K., Long, Z. -F., and Cen, S. (1999b), "A new nine DOF triangular element for analysis of thick and thin plates", *Computational Mechanics*, Vol. 24, No. 5, pp.408-417.

Spilker, R.L., (1982) "Invariant 8-node hybrid stress element for thin and moderately thick plates", *International Journal for Numerical Methods in Engineering*, Vol.18, pp. 1153-1178.

Spilker, R.L. and Munir, N. I., (1980) "A serendipity cubic-displacement hybrid-stress for thin and moderately thick plate", *International Journal for Numerical Methods in Engineering*, Vol.15, pp. 1261-1278.

Taylor, R. L. and Auricchio, F., (1993) "Linked interpolation for Reissner-Mindlin plate elements: Part II—A simple triangle", *International Journal for Numerical Methods in Engineering*, Vol.36 No.18, pp. 3057-3066.

Wang, C. M., Wang, Y. C., Reddy, J. N. and Thevendran, V., (2002) "Improved computation of stress resultants in the p-Ritz method", *Journal of Engineering Mechanics-ASCE*, Vol.128 No.2, pp. 249-257.

Ye, K. S. and Yuan, S., (2002) "Analysis of shells by finite element method of lines (II): Numerical examples", *Engineering Mechanics*, Vol.19 No.5, pp. 16-23. (in Chinese)

Yuan, S., (1993) *The finite element method of lines: Theory and applications*. Science Press: Beijing & New York.

Yuan, S., Jin, Y. and Williams, F. W., (1998) "Bending analysis of Mindlin plates by extended Kantorovich method", *Journal of Engineering Mechanics-ASCE*, Vol.124 No.12, pp. 1339-1345.

Zhang, H. X. and Kuang, J. S., (2007) "Eight-node Reissner-Mindlin plate element based on boundary interpolation using Timoshenko beam function", *International Journal for Numerical Methods in Engineering*, Vol.69, pp. 1345-1373.

Zienkiewicz, O. C. and Taylor, R. L. (2000), *The Finite Element Method, Vol. 2. Solid Mechanics (5th edn)*. Butterworth-heinemann: Oxford.

Zienkiewicz, O. C., Taylor, R. L. and Too, J. M., (1971) "Reduced integration technique in general analysis of plates and shells", *International Journal for Numerical Methods in Engineering*, Vol.38 No.2, pp. 275-290.

Zienkiewicz, O. C., Xu, Z. N., Zeng, L. F. and Samuelsson, A., (1993) "Linked interpolation for Ressiner-Mindlin plate element: part I- a simple quadrilateral", *International Journal for Numerical Methods in Engineering*, Vol.36 No.18, pp. 3043-3056.

Table I. Twenty three fundamental analytical solutions for the general part of the displacement function and resulting resultant forces

i	1	2	3	4	5	6	7
$-DF_i^0$	x^2	xy	y^2	x^3	x^2y	xy^2	y^3
M_x^0	2	0	2μ	$6x$	$2y$	$2\mu x$	$6\mu y$
M_y^0	2μ	0	2	$6\mu x$	$2\mu y$	$2x$	$6y$
M_{xy}^0	0	$1-\mu$	0	0	$2(1-\mu)x$	$2(1-\mu)y$	0
T_x^0	0	0	0	6	0	2	0
T_y^0	0	0	0	0	2	0	6

i	8	9	10	11
$-DF_i^0$	x^3y	xy^3	x^4-y^4	$6x^2y^2-x^4-y^4$
$-DF_i^0$	$6xy$	$6\mu xy$	$12(x^2-\mu y^2)$	$12(1-\mu)(y^2-x^2)$
M_x^0	$6\mu xy$	$6xy$	$-12(y^2-\mu x^2)$	$12(1-\mu)(x^2-y^2)$
M_y^0	$3(1-\mu)x^2$	$3(1-\mu)y^2$	0	$24(1-\mu)xy$
M_{xy}^0	$6y$	$6y$	$24x$	0
T_x^0	$6x$	$6x$	$-24y$	0

i	12	13	14
$-DF_i^0$	$x^3y^2-xy^4$	$5x^3y^2-x^5$	$x^2y^3-x^4y$
M_x^0	$6xy^2+\mu(2x^3-12xy^2)$	$10\mu x^3-20\,x^3+30\,xy^2$	$6\mu x^2y+2y^3-12x^2y$
M_y^0	$6\mu xy^2+2x^3-12xy^2$	$10x^3+\mu(-20\,x^3+30\,xy^2)$	$6x^2y+\mu(2y^3-12x^2y)$
M_{xy}^0	$(1-\mu)(6x^2y-4y^3)$	$30(1-\mu)x^2y$	$(1-\mu)(6xy^2-4x^3)$
T_x^0	$6(x^2-y^2)$	$-30x^2+30y^2$	$-12xy$
T_y^0	$-12xy$	$60xy$	$6(-x^2+y^2)$

i	15	16	17
$-DF_i^0$	$5x^2y^3-y^5$	x^5y-xy^5	$10x^3y^3-3x^5y-3xy^5$
M_x^0	$10y^3+\mu(-20\,y^3+30\,x^2y)$	$-20\mu xy^3+20x^3y$	$60(1-\mu)(xy^3-x^3y)$
M_y^0	$10\mu y^3-20\,y^3+30\,x^2y$	$-20xy^3+20\mu x^3y$	$60(1-\mu)(x^3y-xy^3)$
M_{xy}^0	$30(1-\mu)xy^2$	$5(1-\mu)(x^4-y^4)$	$-15(1-\mu)(x^4-6x^2y^2+y^4)$
T_x^0	$60xy$	$60x^2y-20y^3$	0
T_y^0	$30x^2-30y^2$	$20x^3-60xy^2$	0

i	18	19
$-DF_i^0$	$x^6-10x^4y^2+5x^2y^4$	$y^6-10x^2y^4+5x^4y^2$
M_x^0	$30x^4-120x^2y^2+10y^4+\mu(-20\,x^4+60\,x^2y^2)$	$-20\,y^4+60\,x^2y^2+\mu(30y^4-120x^2y^2+10x^4)$
M_y^0	$-20\,x^4+60x^2y^2+\mu(30x^4-120x^2y^2+10y^4)$	$30y^4-120x^2y^2+10x^4+\mu(-20y^4+60\,x^2y^2)$
M_{xy}^0	$40(1-\mu)(-2x^3y+xy^3)$	$40(1-\mu)(-2xy^3+x^3y)$
T_x^0	$40x^3-120xy^2$	$40x^3-120xy^2$
T_y^0	$40y^3-120x^2y$	$40y^3-120x^2y$

i	20	21
$-DF_i^0$	$21x^5y^2-2x^7-7xy^6$	$35x^4y^3-y^7-14x^6y$
M_x^0	$42(-2x^5+10x^3y^2)+42\mu(x^5-5xy^4)$	$420(-x^4y+x^2y^3)+42\mu(5x^4y-y^5)$
M_y^0	$42(x^5-5xy^4)+42\mu(-2x^5+10x^3y^2)$	$42(5x^4y-y^5)+420\mu(-x^4y+x^2y^3)$
M_{xy}^0	$42(1-\mu)(5x^4y-y^5)$	$84(1-\mu)(5x^3y^2-x^5)$
T_x^0	$-210(x^4-6x^2y^2+y^4)$	$-840(x^3y-xy^3)$
T_y^0	$840(x^3y-xy^3)$	$-210(x^4-6x^2y^2+y^4)$

i	22	23
$-DF_i^0$	$35x^3y^4-x^7-14xy^6$	$21x^2y^5-2y^7-7x^6y$
M_x^0	$42(5xy^4-x^5)+420\mu(-xy^4+x^3y^2)$	$42(y^5-5x^4y)+42\mu(-2y^5+10x^2y^3)$
M_y^0	$420(-xy^4+x^3y^2)+42\mu(5xy^4-x^5)$	$42(-2y^5+10x^2y^3)+42\mu(y^5-5x^4y)$
M_{xy}^0	$84(1-\mu)(5x^2y^3-y^5)$	$42(1-\mu)(5xy^4-x^5)$
T_x^0	$-210(x^4-6x^2y^2+y^4)$	$-840(x^3y-xy^3)$
T_y^0	$840(x^3y-xy^3)$	$-210(x^4-6x^2y^2+y^4)$

Table II. Two analytical solutions for the displacement function f and the resulting resultant forces

$\mathbf{R}_j^f$	j =1	j =2
M_{xj}^f	$(1-\mu)mne^{mx+ny-a_0}$	$(1-\mu)\left[(nx-my)mn+n^2-m^2\right]e^{mx+ny-a_0}$
M_{yj}^f	$-(1-\mu)mne^{mx+ny-a_0}$	$-(1-\mu)\left[(nx-my)mn+n^2-m^2\right]e^{mx+ny-a_0}$
M_{xyj}^f	$\frac{1}{2}(1-\mu)(n^2-m^2)e^{mx+ny-a_0}$	$\frac{1}{2}(1-\mu)\left[-4mn+(nx-my)(n^2-m^2)\right]e^{mx+ny-a_0}$
T_{xj}^f	$\frac{C}{D}ne^{mx+ny-a_0}$	$\frac{C}{D}\left[(nx-my)n-m\right]e^{mx+ny-a_0}$
T_{yj}^f	$-\frac{C}{D}me^{mx+ny-a_0}$	$-\frac{C}{D}\left[(nx-my)m+n\right]e^{mx+ny-a_0}$

Table III. Clamped square plate: Dimensionless results of central deflection w_c /(qL^4 /100D) and moment M_c /(qL^2/10D) obtained by element HDF-P8-23β (Example 4.3)

h/L	Mesh type	Mesh density 1×1	2×2	4×4	8×8	16×16	Analytical solutions
		w_c /(qL^4 /100D)					
10^{-30}~0.001	Mesh A-regular	0.12505	0.12636	0.12652	0.12653	0.12653	0.1265
	Mesh B-distorted	–	0.12634	0.12652	0.12653	0.12653	
	Mesh C-distorted	–	0.12628	0.12652	0.12653	0.12653	
0.01	Mesh A-regular	0.12530	0.12662	0.12677	0.12678	0.12678	0.1267
	Mesh B-distorted	–	0.12659	0.12677	0.12678	0.12678	
	Mesh C-distorted	–	0.12654	0.12677	0.12678	0.12678	
0.1	Mesh A-regular	0.14944	0.15072	0.15066	0.15055	0.15049	0.1499
	Mesh B-distorted	–	0.15071	0.15067	0.15056	0.15049	
	Mesh C-distorted	–	0.15066	0.15069	0.15057	0.15050	
		M_c /(qL^2 /10D)					
10^{-30}~0.001	Mesh A-regular	0.24196	0.22902	0.22908	0.22905	0.22905	0.2291
	Mesh B-distorted	–	0.22069	0.22895	0.22903	0.22905	
	Mesh C-distorted	–	0.21864	0.22879	0.22901	0.22905	
0.01	Mesh A-regular	0.24187	0.22909	0.22912	0.22910	0.22909	0.2291
	Mesh B-distorted	–	0.22137	0.22899	0.22908	0.22909	
	Mesh C-distorted	–	0.21935	0.22887	0.22907	0.22909	
0.1	Mesh A-regular	0.23827	0.23159	0.23214	0.23209	0.23203	0.231
	Mesh B-distorted	–	0.23118	0.23217	0.23210	0.23203	
	Mesh C-distorted	–	0.23061	0.23218	0.23211	0.23204	

Table IV. SS2 square plate: Dimensionless results of central deflection w_c /(qL^4 /100D) and moment M_c /(qL^2/10D) obtained by element HDF-P8-23β (Example 4.3)

h/L	Mesh type	Mesh density 1×1	2×2	4×4	8×8	16×16	Analytical solutions
		w_c /(qL^4 /100D)					
10^{-30}~0.001	Mesh A-regular	0.40579	0.40620	0.40623	0.40623	0.40623	0.4062
	Mesh B-distorted	–	0.40626	0.40623	0.40623	0.40623	
	Mesh C-distorted	–	0.40628	0.40624	0.40623	0.40623	
0.01	Mesh A-regular	0.40601	0.40641	0.40644	0.40644	0.40644	0.4064
	Mesh B-distorted	–	0.40646	0.40644	0.40644	0.40644	
	Mesh C-distorted	–	0.40648	0.40644	0.40644	0.40644	
0.1	Mesh A-regular	0.42697	0.42724	0.42728	0.42728	0.42728	0.4273
	Mesh B-distorted	–	0.42725	0.42728	0.42728	0.42728	
	Mesh C-distorted	–	0.42726	0.42728	0.42728	0.42728	
		M_c /(qL^2 /10D)					
10^{-30}~0.001	Mesh A-regular	0.49074	0.47909	0.47888	0.47887	0.47886	
	Mesh B-distorted	–	0.47384	0.47863	0.47883	0.47886	
	Mesh C-distorted	–	0.47263	0.47841	0.47882	0.47886	
0.01	Mesh A-regular	0.49060	0.47908	0.47888	0.47886	0.47886	0.4789
	Mesh B-distorted	–	0.47416	0.47866	0.47884	0.47886	
	Mesh C-distorted	–	0.47298	0.47849	0.47884	0.47886	
0.1	Mesh A-regular	0.48279	0.47869	0.47884	0.47886	0.47886	
	Mesh B-distorted	–	0.47818	0.47883	0.47886	0.47886	
	Mesh C-distorted	–	0.47786	0.47883	0.47886	0.47886	

Table V. SS1 square plate: Dimensionless results of central deflection w_c /(qL^4 /100D) and moment M_c /(qL^2/10D) obtained by element HDF-P8-23β and HDF-P8-SS1 (Example 4.3)

h/L	Mesh type	Mesh density 1×1	2×2	4×4	8×8	16×16	Analytical solutions
			w_c /(qL^4 /100D)				
10^{-30}~0.001	Mesh A-regular	0.40925	0.40698	0.40678	0.40658	0.40631	0.4062
	Mesh B-distorted	–	0.40691	0.40656	0.40648	0.40634	
	Mesh C-distorted	–	0.40695	0.40657	0.40643	0.40637	
0.1	Mesh A-regular	0.47047	0.46388	0.46220	0.46186	0.46187	0.4617
	Mesh B-distorted	–	0.46265	0.46191	0.46181	0.46187	
	Mesh C-distorted	–	0.46223	0.46182	0.46181	0.46189	
			M_c /(qL^2 /10D)				
10^{-30}~0.001	Mesh A-regular	0.44896	0.48035	0.47937	0.47917	0.47893	0.4789
	Mesh B-distorted	–	0.47518	0.47896	0.47906	0.47895	
	Mesh C-distorted	–	0.47420	0.47882	0.47900	0.47898	
0.1	Mesh A-regular	0.45202	0.51146	0.50995	0.50972	0.50974	0.5096
	Mesh B-distorted	–	0.50959	0.50970	0.50967	0.50974	
	Mesh C-distorted	–	0.50909	0.50963	0.50968	0.50976	

Table VI. Results of deflections and principal moments

at the center of Morley's 30° skew plate (L/h=1000)

Mesh $N\times N$	4×4	8×8	16×16	32×32	Morley's solutions for thin plate
(a) Central deflection $w_o/(qL^4/1000D)$					
QH8-39β	0.416	0.422	0.420	0.417	0.408
HDF-P4-11β	0.462	0.426	0.419	0.416	
S8R	0.181	0.279	0.326	0.356	
Present	**0.423**	**0.419**	**0.417**	**0.415**	
(b) Central max principal moment $M_{max}/(qL^2/100D)$					
QH8-39β	1.911	1.936	1.938	1.933	1.910
HDF-P4-11β	2.197	1.873	1.935	1.930	
S8R	1.241	1.517	1.671	1.757	
Present	**1.932**	**1.902**	**1.925**	**1.925**	
(c) Central min principal moment $M_{min}/(qL^2/100D)$					
QH8-39β	0.966	1.136	1.131	1.122	1.080
HDF-P4-11β	1.399	1.104	1.169	1.125	
S8R	0.492	0.705	0.802	0.889	
Present	**1.121**	**1.109**	**1.119**	**1.112**	

- QH8-39β (Li *et al*. 2015);
- HDF-P4-11β (Cen *et al*. 2014);
- S8R (*Abaqus* 2009);
- Morley (1963)

Table VII. Results of deflections and principal moments

at the center of Morley's 30° skew plate (L/h=100)

Mesh $N\times N$	4×4	8×8	16×16	32×32	Morley's solutions for thin plate	3D Solution
(a) Central deflection $w_o/(qL^4/1000D)$						
QH8-39β	0.418	0.425	0.425	0.424	0.408	0.423
HDF-P4-11β	0.463	0.427	0.421	0.420		
S8R	0.262	0.328	0.377	0.406		
Present	**0.427**	**0.425**	**0.424**	**0.424**		
(b) Central max principal moment $M_{max}/(qL^2/100D)$						
QH8-39β	1.919	1.941	1.950	1.954	1.910	
HDF-P4-11β	2.198	1.882	1.942	1.937		
S8R	1.717	1.705	1.828	1.904		
Present	**1.956**	**1.931**	**1.949**	**1.954**		
(c) Central min principal moment $M_{min}/(qL^2/100D)$						
QH8-39β	0.963	1.134	1.143	1.143	1.080	
HDF-P4-11β	1.400	1.108	1.157	1.130		
S8R	0.777	0.818	0.964	1.076		
Present	**1.148**	**1.144**	**1.146**	**1.144**		

- QH8-39β (Li *et al*. 2015);
- HDF-P4-11β (Cen *et al*. 2014);
- S8R (*Abaqus* 2009);
- Morley (1963);
- 3D (Babuška and Scapolla 1989)

Table VIII. Normalized center deflection w_c / w_{ref} and moments M_c / M_{ref} of simply-supported (SS1) circular plates subjected to a uniform load

Mesh N	1	3	12	48	Analytical
(a) h/R=0.02 (h=0.1)			w_c / w_{ref}		
DONEA	0.9690	0.9980	0.9997	—	1.0000
Kuang	—	0.9945	0.9967	0.9992	(the reference
QH-39β	—	1.0276	1.0075	1.0025	value is 39831.5)
S8R	0.9524	1.0070	0.9998	1.0000	
HDF-P4-11β	—	1.0242	1.0065	1.0017	
Present	**1.0002**	**1.0008**	**1.0001**	**1.0000**	
			M_c/ M_{ref}		
Kuang	—	0.9864	0.9922	0.9961	1.0000
QH-39β	—	0.9149	0.9922	0.9990	(the reference
S8R	1.1000	1.2424	1.0087	1.0027	value is 5.15625)
HDF-P4-11β	—	1.0262	1.0046	1.0012	
Present	**1.0152**	**1.0041**	**1.0003**	**1.0000**	
(b) h/R=0.2 (h=1)			w_c / w_{ref}		
Kuang	—	0.9907	0.9975	0.9988	1.0000
QH-39β	—	1.0841	1.0312	1.0120	(the reference
S8R	0.9594	1.0012	0.9999	1.0000	value is 41.5994)
HDF-P4-11β	—	1.0206	1.0048	1.0010	
Present	**1.0002**	**1.0010**	**1.0001**	**1.0000**	
			M_c/ M_{ref}		
Kuang	—	0.9864	0.9922	0.9981	1.0000
QH-39β	—	0.8408	0.9920	0.9990	(the reference
S8R	1.1468	1.0771	1.0156	1.0040	value is 5.15625)
HDF-P4-11β	—	1.0170	1.0030	1.0007	
Present	**1.0060**	**1.0008**	**1.0000**	**1.0000**	

- DONEA (Donea and Lamain 1987);
- Kuang (Zhang and Kuang 2007);
- QH8-39β (Li *et al*. 2015);
- HDF-P4-11β (Cen *et al*. 2014);
- S8R (*Abaqus* 2009);

Table IX. Normalized center deflection w_c / w_{ref} and moments M_c / M_{ref} of clamped circular plates subjected to a uniform load

Mesh N	1	3	12	48	Analytical
(a) h/R=0.02 (h=0.1)			w_c / w_{ref}		
DONEA	0.2960	1.0130	1.0020	—	1.0000
S8R	0.1042	0.8621	0.9619	0.9971	(the reference
Kuang	—	0.9620	0.9957	0.9998	value is 9783.48)
HDF-P4-11β	—	0.7985	0.9484	0.9871	
Present	**0.9965**	**0.9983**	**0.9999**	**1.0000**	
			M_c/ M_{ref}		
S8R	0.1599	0.8169	1.0082	1.0083	1.0000
Kuang	—	0.9901	0.9951	0.9999	(the reference
HDF-P4-11β	—	0.9151	0.9727	0.9933	value is 2.03125)
Present	**1.0557**	**1.0050**	**1.0008**	**1.0001**	
(b) h/R=0.2 (h=1)			w_c / w_{ref}		
S8R	0.9698	0.9992	0.9993	1.0000	1.0000
Kuang	—	0.9931	0.9955	0.9974	(the reference
HDF-P4-11β	—	0.8200	0.9512	0.9871	value is 11.5513)
Present	**0.9984**	**0.9985**	**0.9999**	**1.0000**	
			M_c/ M_{ref}		
S8R	1.5142	1.1410	1.0390	1.0101	1.0000
Kuang	—	0.9951	0.9992	0.9995	(the reference
HDF-P4-11β	—	0.8924	0.9686	0.9918	Value is 2.03125)
Present	**1.0310**	**1.0008**	**1.0000**	**1.0000**	

- DONEA (Donea and Lamain 1987);
- Kuang (Zhang and Kuang 2007);
- QH8-39β (Li *et al*. 2015);
- HDF-P4-11β (Cen *et al*. 2014);
- S8R (*Abaqus* 2009);

Table X. The dimensionless results of displacements and resultants at certain positions for the SFSF square plate

	Mesh $N\times N$	2×2	4×4	8×8	12×12	16×16	FEMOL	Kant
$\frac{w_C \cdot D}{qa^4}$	HDF-P4-FREE	—	0.01311	0.01311	0.01311	0.01311		
	S8R	0.01311	0.01311	0.01311	0.01311	0.01311	0.01311	0.0131
	Present	**0.01311**	**0.01311**	**0.01311**	**0.01311**	**0.01311**		
$\frac{w_D \cdot D}{qa^4}$	HDF-P4-FREE	—	0.01507	0.01507	0.01507	0.01507		
	S8R	0.01512	0.01507	0.01507	0.01507	0.01507	0.01507	0.0150
	Present	**0.01507**	**0.01507**	**0.01507**	**0.01507**	**0.01507**		
$\frac{M_{xC}}{qa^2}$	HDF-P4-FREE	—	0.02650	0.02675	0.02680	0.02681		
	S8R	0.02851	0.02731	0.02695	0.02688	0.02686	0.02683	0.0268
	Present	**0.02576**	**0.02656**	**0.02676**	**0.02680**	**0.02681**		
$\frac{M_{yC}}{qa^2}$	HDF-P4-FREE	—	0.1229	0.1226	0.1225	0.1225		
	S8R	0.1273	0.1237	0.1228	0.1226	0.1226	0.1225	0.1220
	Present	**0.1235**	**0.1227**	**0.1225**	**0.1225**	**0.1225**		
$\frac{M_{yD}}{qa^2}$	HDF-P4-FREE	—	0.1304	0.1304	0.1304	0.1304		
	S8R	0.1361	0.1322	0.1312	0.1309	0.1308	0.1304	0.130
	Present	**0.1308**	**0.1305**	**0.1304**	**0.1304**	**0.1304**		
$\frac{M_{xyA}}{qa^2}$	HDF-P4-FREE	—	0.00000	0.00000	0.00000	0.00000		
	S8R	0.01676	0.01795	0.01415	0.01124	0.00910	NA	NA
	Present	**0.00000**	**0.00000**	**0.00000**	**0.00000**	**0.00000**		
$\frac{T_{yB}}{qa}$	HDF-P4-FREE	—	0.4381	0.4552	0.4609	0.4634		
	S8R	0.4286	0.4286	0.4678	0.4679	0.4679	0.4679	0.463
	Present	**0.4431**	**0.4612**	**0.4659**	**0.4671**	**0.4675**		
$\frac{T_{xD}}{qa}$	HDF-P4-FREE	—	0.00000	0.00000	0.00000	0.00000		
	S8R	0.01362	0.04750	0.03875	0.03053	0.02468	NA	NA
	Present	**0.00000**	**0.00000**	**0.00000**	**0.00000**	**0.00000**		

- FEMOL (Yuan 1993);
- Kant (Kant and Gadgil 2002; Kant and Hinton 1983);
- HDF-P4-FREE (Shang *et al*. 2015);
- S8R (*Abaqus* 2009);

Table XI. The dimensionless results of displacements and resultants at certain positions for the SS*SS* square plate

	Mesh $N\times N$	2×2	4×4	8×8	12×12	16×16	Kant
$\frac{w_C \cdot D}{qa^4}$	HDF-P4-SS1	—	0.00410	0.00410	0.00410	0.00411	
	S8R	0.00412	0.00411	0.00411	0.00411	0.00411	0.0041
	Present	**0.00411**	**0.00411**	**0.00411**	**0.00411**	**0.00411**	
$\frac{M_{xC}}{qa^2}$	HDF-P4-SS1	—	0.04806	0.04809	0.04810	0.04811	
	S8R	0.05193	0.04901	0.04834	0.04822	0.04818	0.0481
	Present	**0.04814**	**0.04812**	**0.04813**	**0.04813**	**0.04813**	
$\frac{M_{yC}}{qa^2}$	HDF-P4-SS1	—	0.04821	0.04822	0.04824	0.04825	
	S8R	0.05253	0.04913	0.04848	0.04836	0.04832	0.0482
	Present	**0.04815**	**0.04827**	**0.04827**	**0.04827**	**0.04827**	
$\frac{M_{xyA}}{qa^2}$	HDF-P4-SS1	—	0.00000	0.00000	0.00000	0.00000	
	S8R	-0.02648	–0.02547	–0.01941	–0.01528	–0.01232	NA
	Present	**0.00000**	**0.00000**	**0.00000**	**0.00000**	**0.00000**	
$\frac{T_{yA}}{qa}$	HDF-P4-SS1	—	–5.087	–5.074	–5.047	–5.039	
	S8R	-0.772	–1.325	–2.207	–2.834	–3.289	–5.214
	Present	**-5.504**	**-5.441**	**-5.346**	**-5.252**	**-5.197**	
$\frac{T_{yB}}{qa}$	HDF-P4-SS1	—	0.3076	0.3154	0.3179	0.3208	
	S8R	0.5224	0.3975	0.3394	0.3392	0.3392	0.333
	Present	**0.3415**	**0.3335**	**0.3371**	**0.3383**	**0.3387**	
$\frac{T_{xD}}{qa}$	HDF-P4-SS1	—	0.4226	0.4095	0.3875	0.3697	
	S8R	0.3978	0.3563	0.3708	0.3810	0.3883	0.419
	Present	**0.4178**	**0.4157**	**0.4129**	**0.4133**	**0.4137**	

- Kant (Kant and Gadgil 2002; Kant and Hinton 1983);
- HDF-P4-FREE (Shang *et al*. 2015);
- S8R (*Abaqus* 2009);

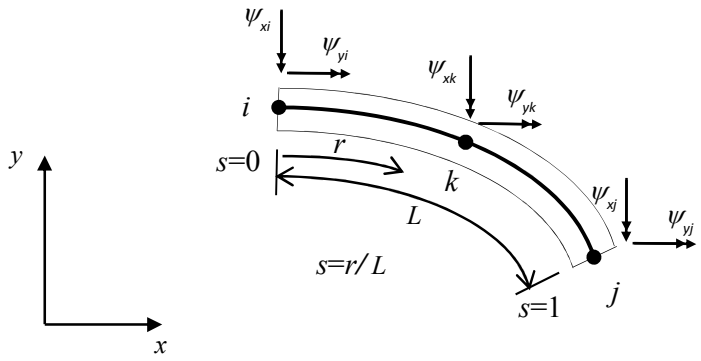

Figure 1. Timoshenko's beam element(curved)

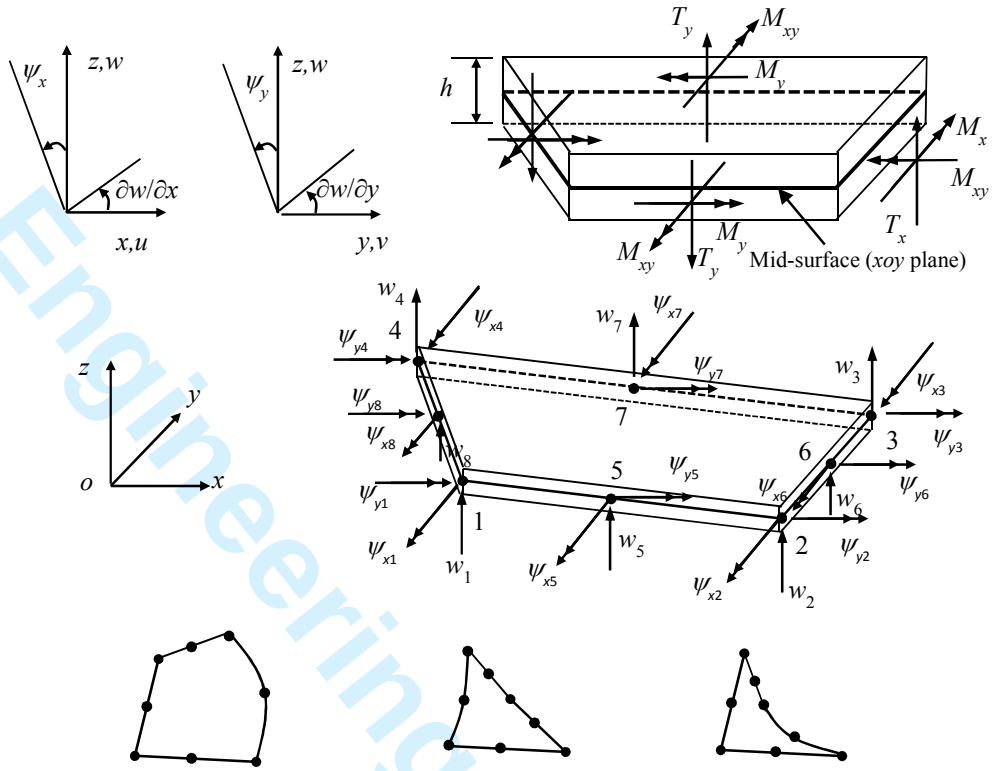

Figure 2. Shape-free 8-node quadrilateral plate bending element

$E = 1000.0$; $\mu = 0.3$; $h = 0.04, 0.4, 4$; $a = 20$; $b = 10$.

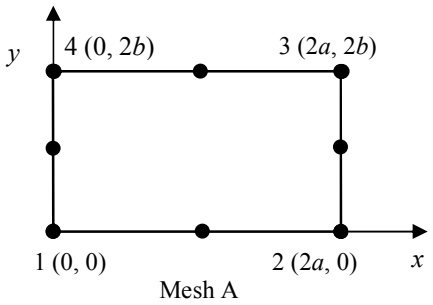

Mesh A

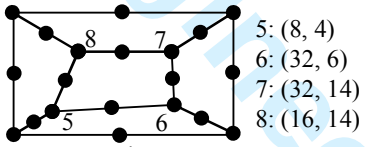

5: (8, 4)
6: (32, 6)
7: (32, 14)
8: (16, 14)

Mesh B

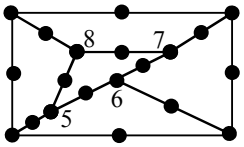

5: (8, 4)
6: (20, 9)
7: (32, 14)
8: (16, 14)

Mesh C

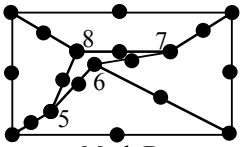

5: (8, 4)
6: (18, 11)
7: (32, 14)
8: (16, 14)

Mesh D

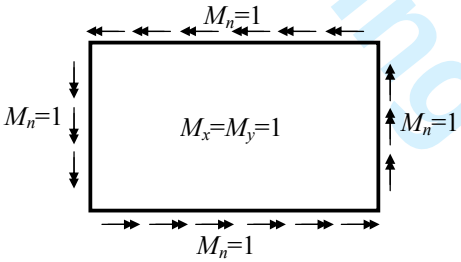

(a) Bending (M_n=1).

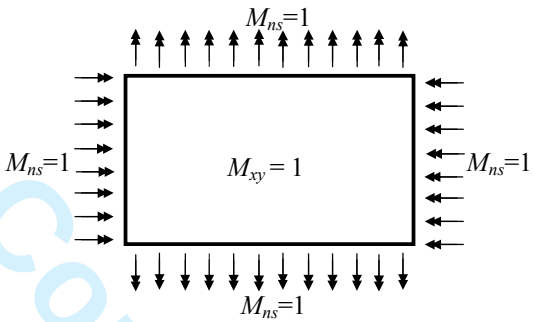

(b) Twist (M_{ns}=1).

BC: w_1=w_2=w_3=0

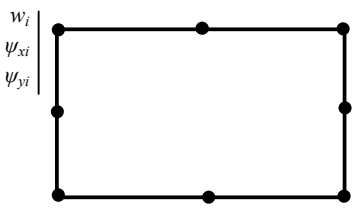

(c) Non-zero constant shear (T_x=Constant, T_y=Constant,).

$$\begin{cases} w_i = a_0 + a_1 x_i + a_2 y_i + a_3 x_i^2 + a_4 x_i y_i + a_5 y_i^2 + a_6 x_i^3 + a_7 x_i^2 y_i + a_8 x_i y_i^2 + a_9 y_i^3 \\ \psi_{xi} = \dfrac{h^2}{2.5(1-\mu)}(3a_6 + a_8) + a_1 + 2a_3 x_i + a_4 y_i + 3a_6 x_i^2 + 2a_7 x_i y_i + a_8 y_i^2 \\ \psi_{yi} = \dfrac{h^2}{2.5(1-\mu)}(a_7 + 3a_9) + a_2 + a_4 x_i + 2a_5 y_i + a_7 x_i^2 + 2a_8 x_i y_i + 3a_9 y_i^2 \end{cases}$$

$$\begin{cases} T_{xi} = \dfrac{Eh^3}{6(1-\mu^2)}(3a_6 + a_8) = \text{Constant} \\ T_{yi} = \dfrac{Eh^3}{6(1-\mu^2)}(a_7 + 3a_9) = \text{Constant} \end{cases}$$

$a_0, \ldots, a_9$ are arbitrary constants, given the nodal deflections and rotations, exact results within the element could be calculated

Figure 3. Patch tests, geometry, loads and meshes

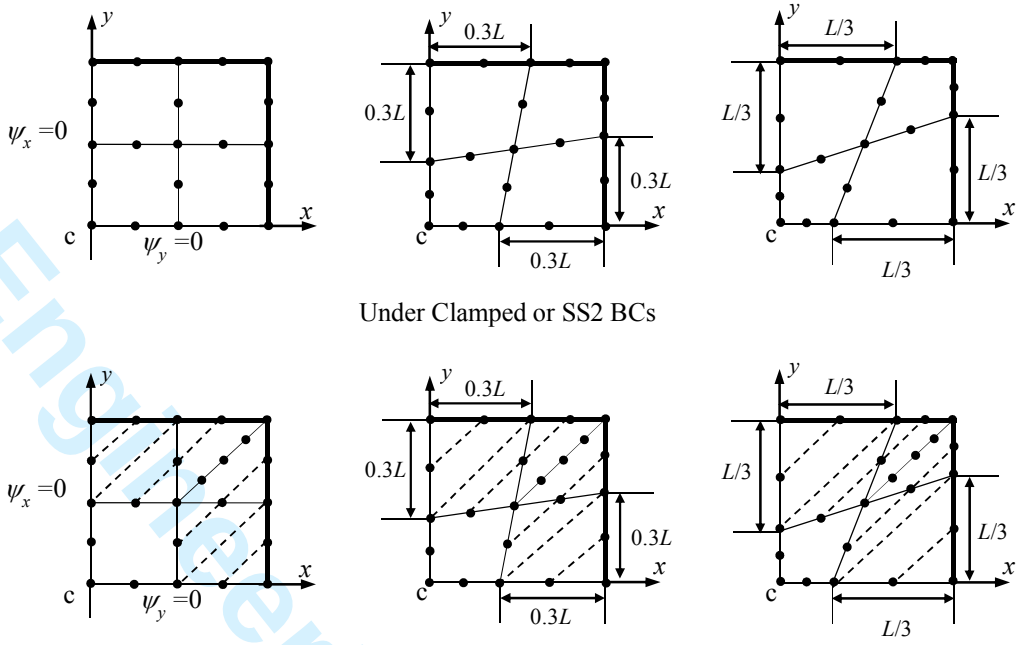

Figure 4. Typical meshes used by a quarter of square plate (c is the central point of plate)

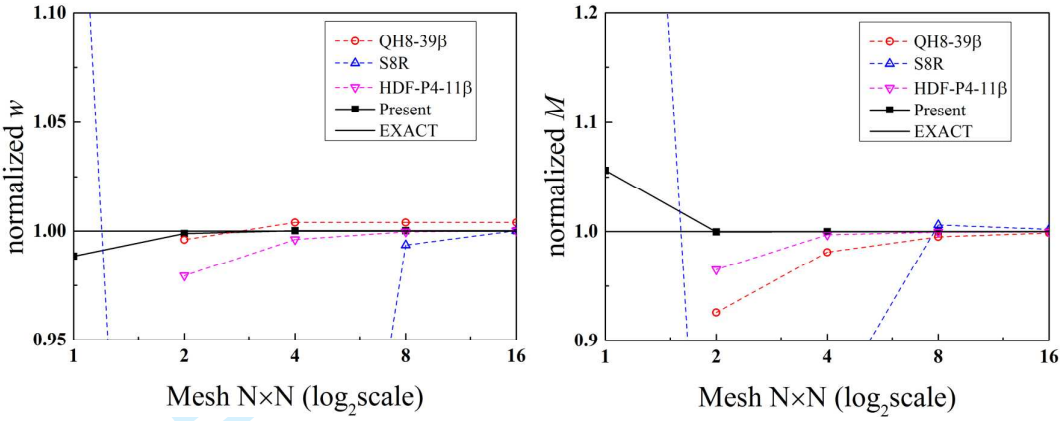

a) h/L=0.001 (thin plate case)

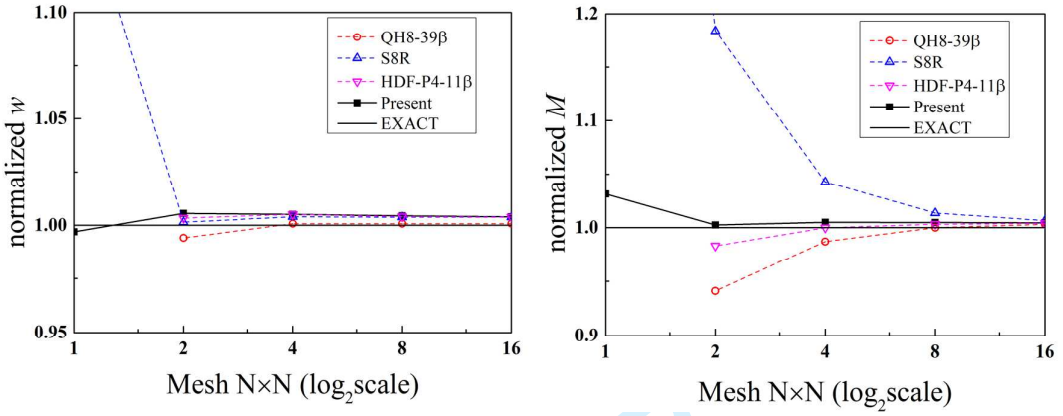

b) h/L=0.1 (thick plate case)

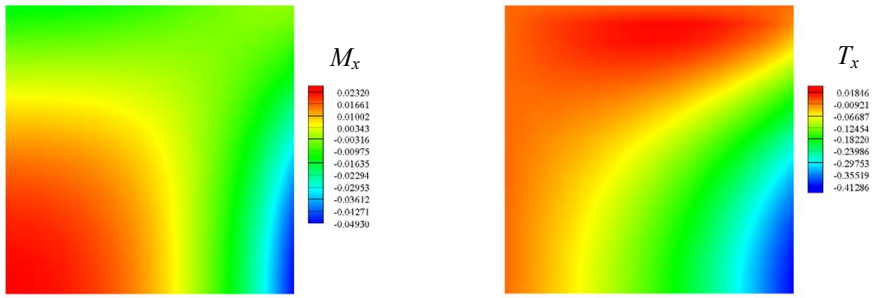

c) Contour plot under h/L=0.1 using Mesh 16×16

Figure 5. Convergence of the central deflections and moments and contour plot for square plates subjected to uniform load (Clamped BC, Mesh A)

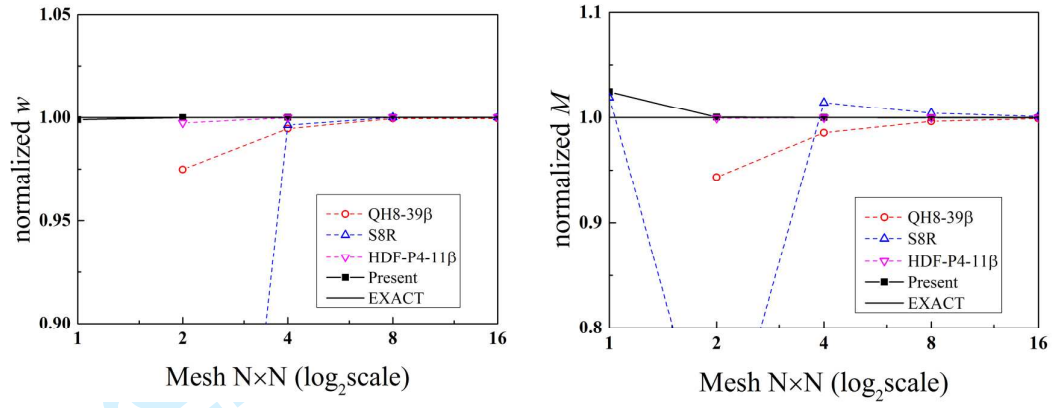

a) h/L=0.001 (thin plate case)

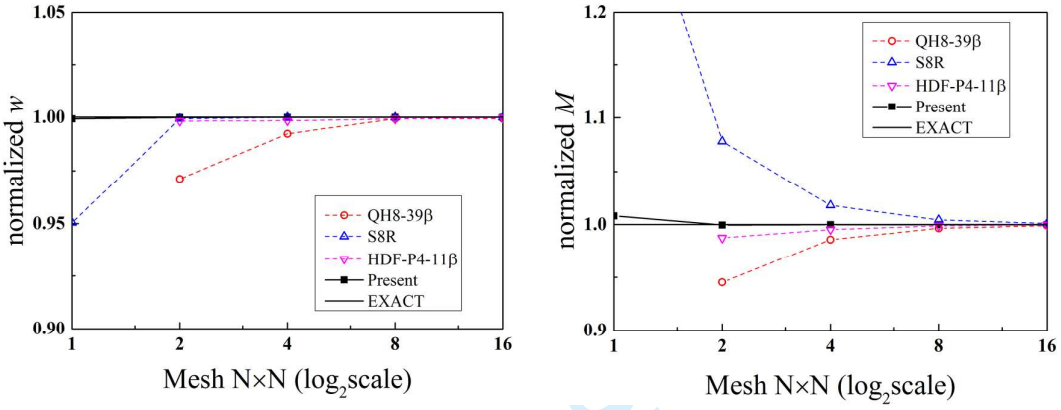

b) h/L=0.1 (thick plate case)

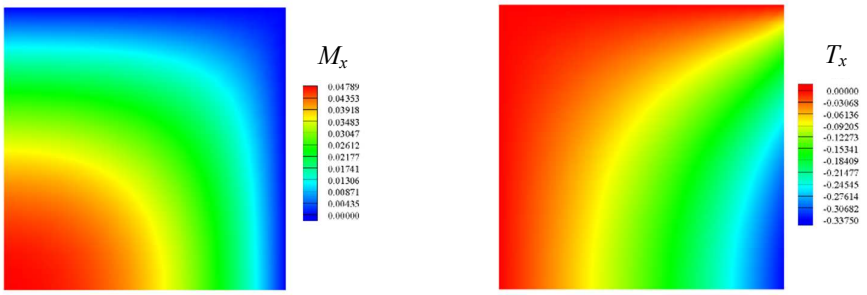

c) Contour plot under h/L=0.1 using Mesh 16×16

Figure 6. Convergence of the central deflections and moments and contour plot for square plates subjected to uniform load (SS2 BC, Mesh A)

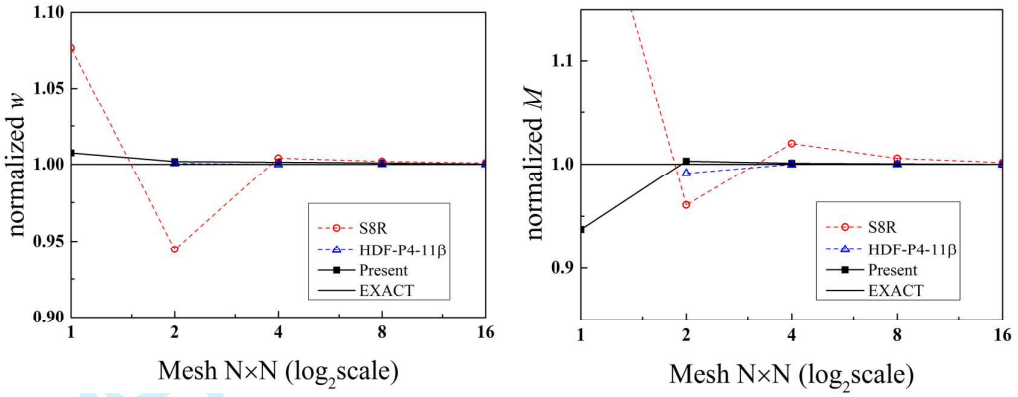

a) h/L=0.001 (thin plate case)

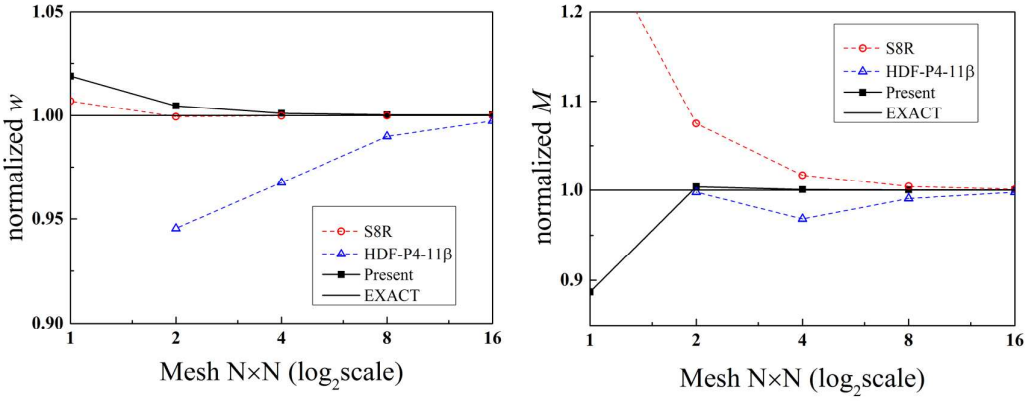

b) h/L=0.1 (thick plate case)

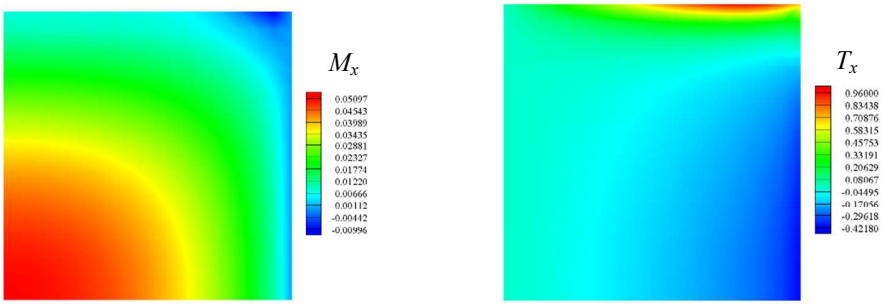

c) Contour plot under h/L=0.1 using Mesh 16×16

Figure 7. Convergence of the central deflections and moments and contour plot for square plates subjected to uniform load (SS1 BC, Mesh A)

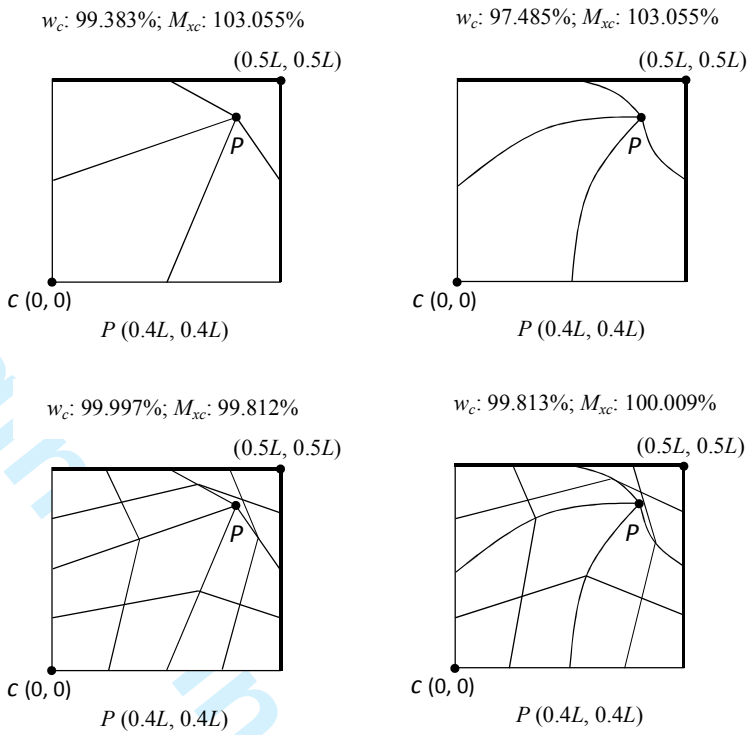

Figure 8. Distorted meshes and normalized results for a quarter of clamped square plate (omitting middle nodes)

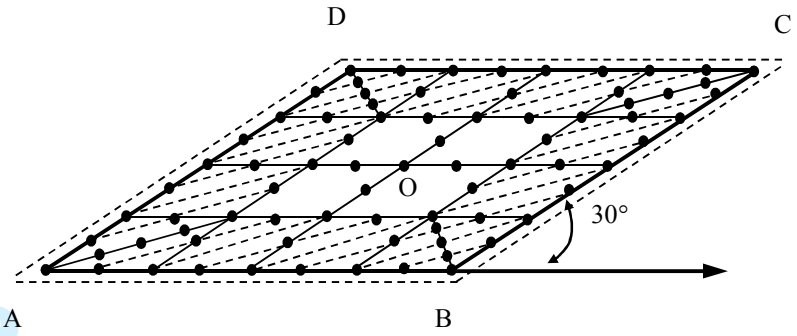

E=10.92; μ=0.3; h=0.1 and 1;
L=100; L/h=1000; 100
Uniform load q=1

Displacement BCs:
w=0 along ABCD


HDF-P8-23β


HDF-P8-SS1

Figure 9. Mesh 4×4 for Morley's 30° skew plate

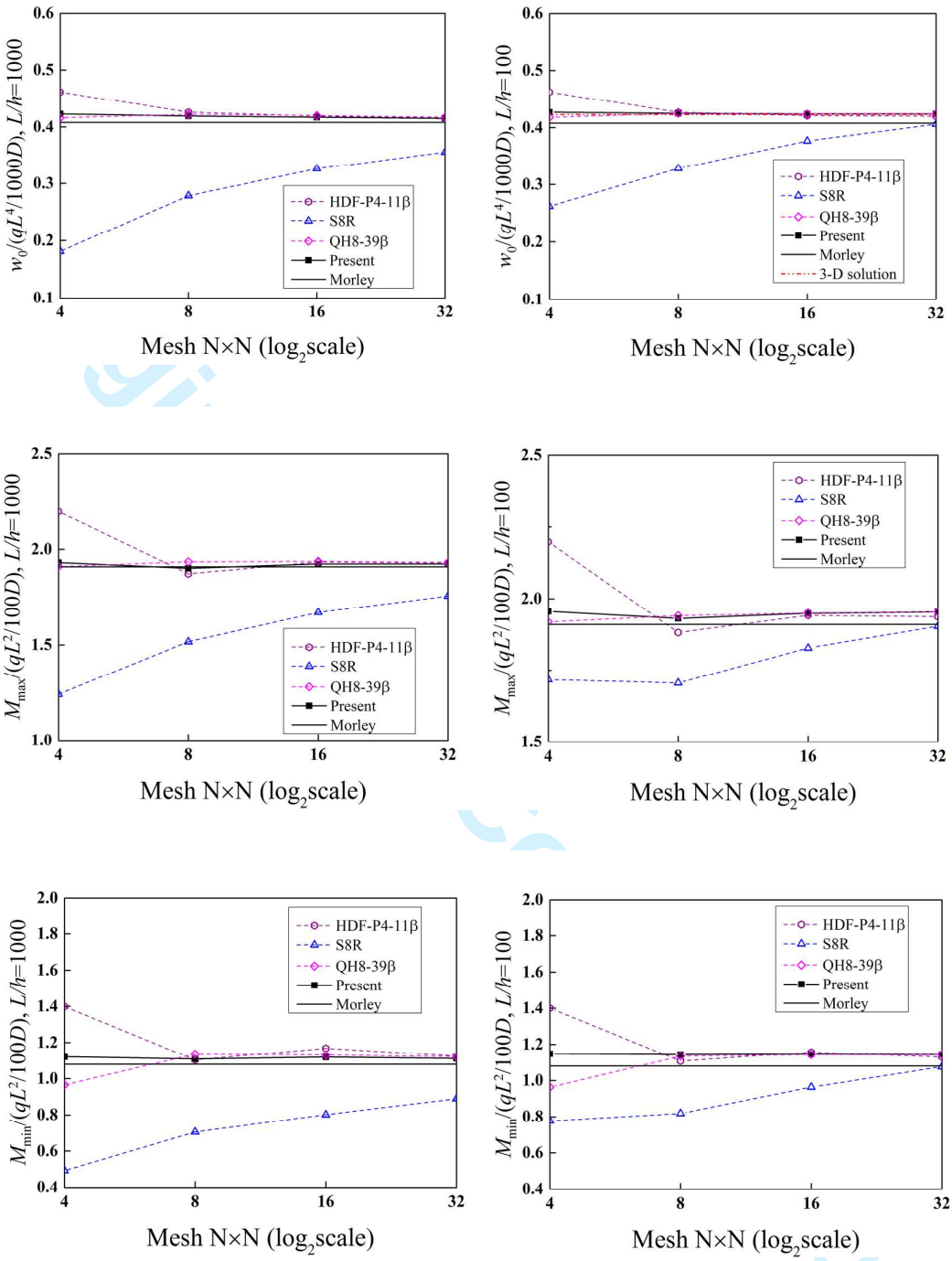

Figure 10. Convergence test for central deflections and principle moments of Morley's 30° skew plate

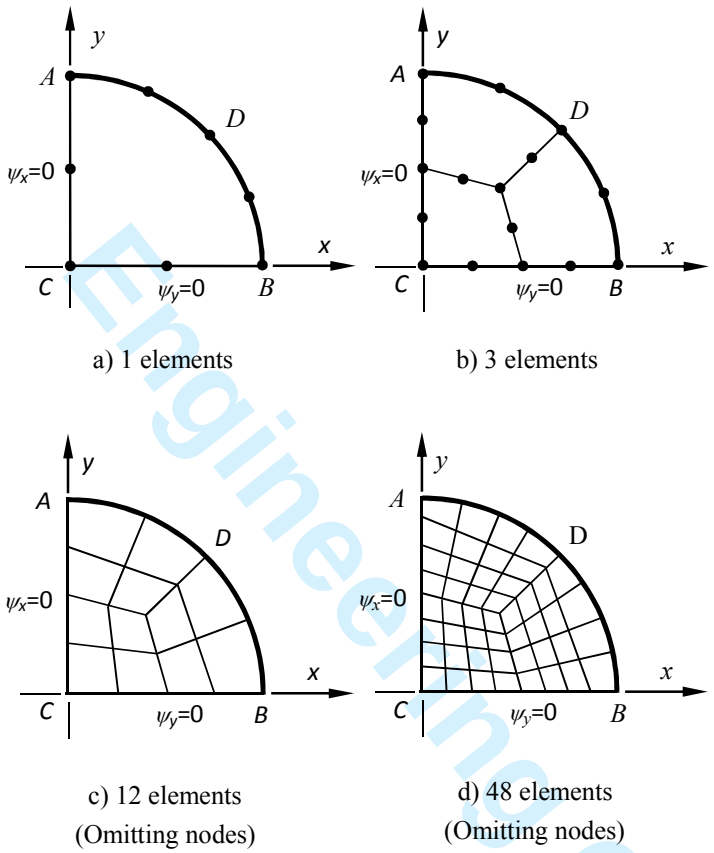

a) 1 elements b) 3 elements

c) 12 elements (Omitting nodes) d) 48 elements (Omitting nodes)

C is the central point of the plate
Radius R=5
E=10.92; μ=0.3;
Uniform loading: q=1
Displacement BCs:
w=0 (SS1) along A-D-B
$w=\psi_n=\psi_s=0$ (Clamped) along A-D-B
Symmetrical conditions
ψ_x =0 along CA
ψ_y =0 along CB

Figure 11. Circular plate problem

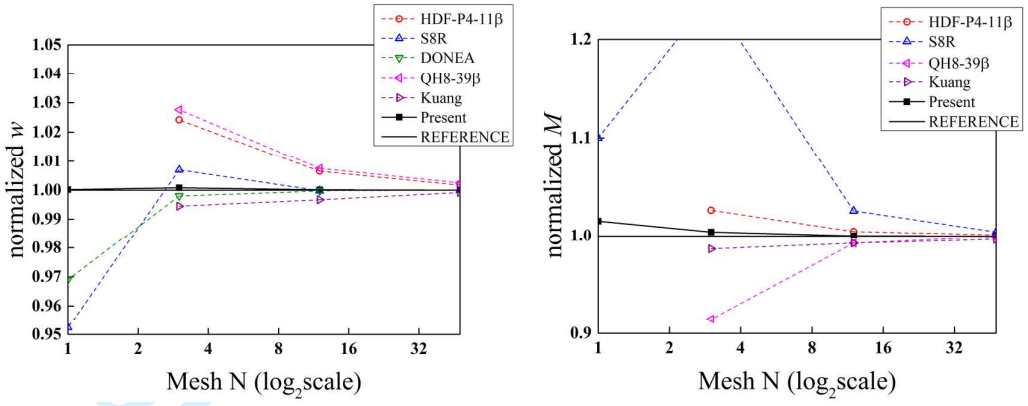

a) h/R=0.02 (thin plate case)

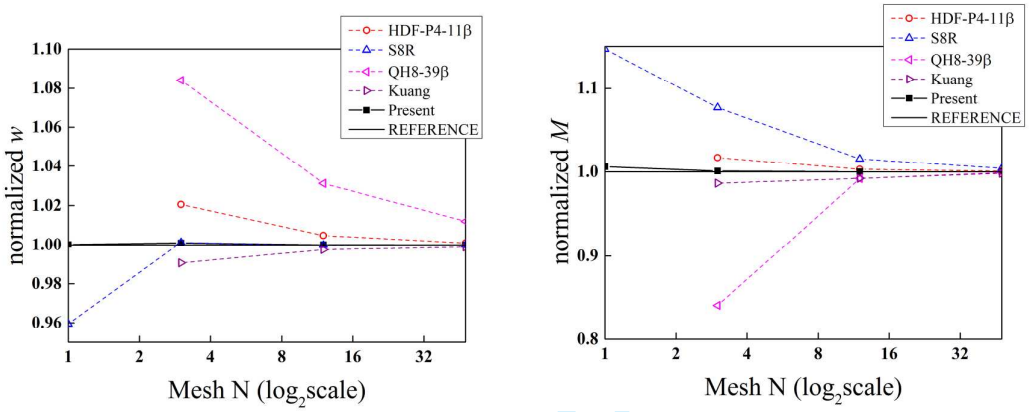

b) h/R=0. 2 (thick plate case)

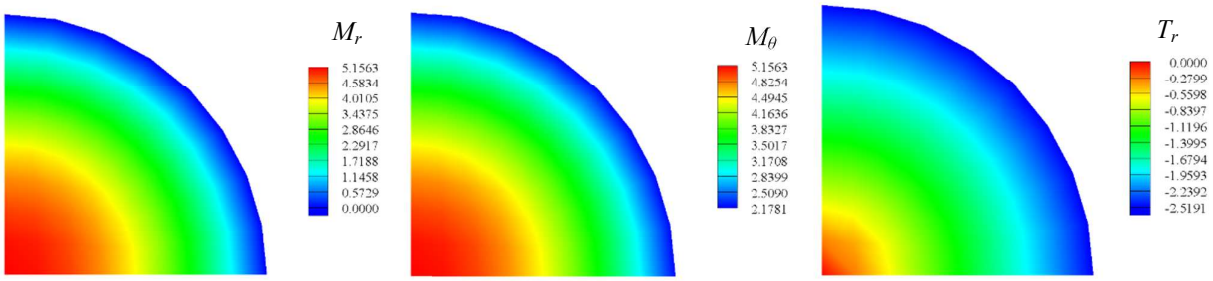

c) Contour plot under h/R=0.2 using 48 elements

Figure 12. Convergence of the central deflections and moments and contour plot for circular plates subjected to uniform load (SS1 BC)

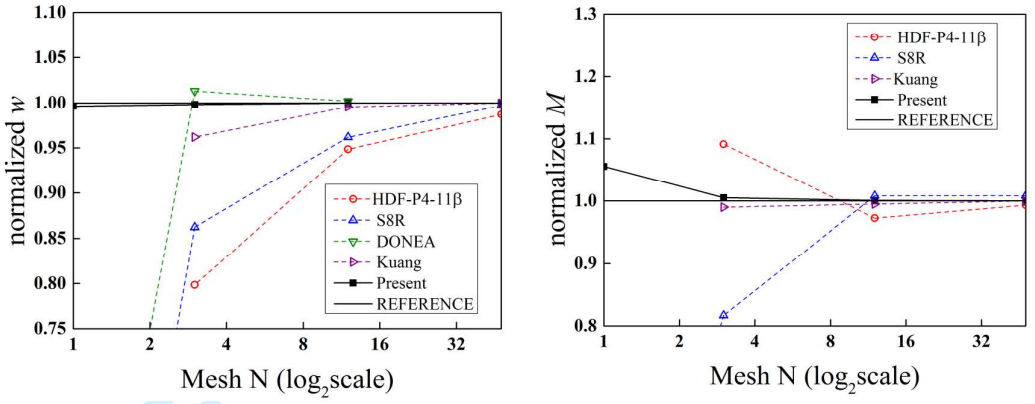

a) h/R=0.02 (thin plate case)

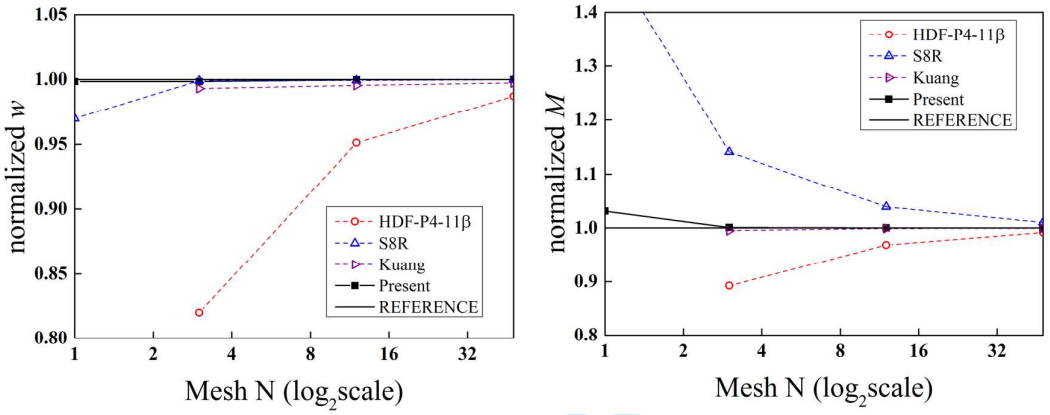

b) h/R=0. 2 (thick plate case)

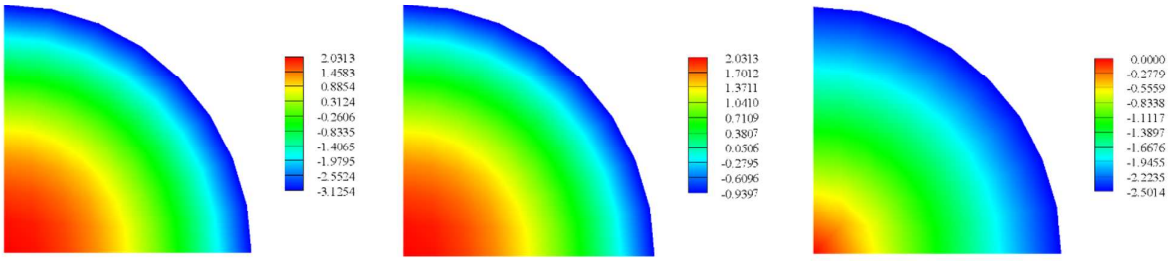

c) Contour plot under h/R=0.2 using 48 elements

Figure 13. Convergence of the central deflections and moments and contour plot for circular plates subjected to uniform load (Clamped BC)

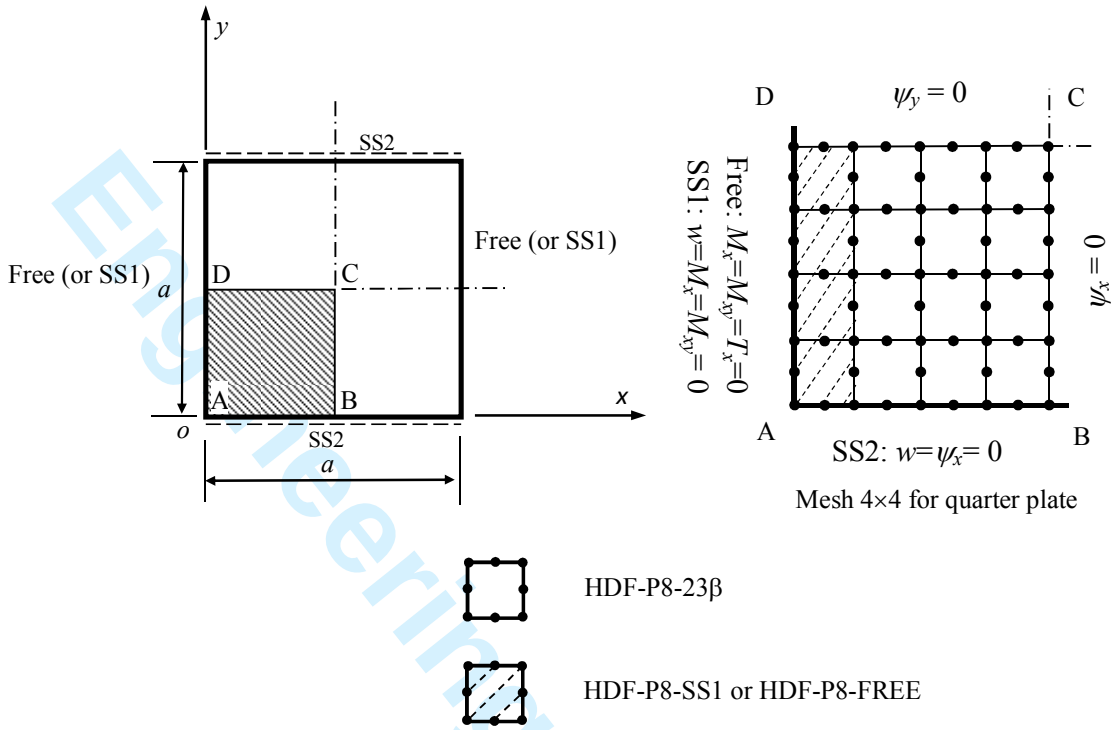

Figure 14. The typical meshes and the arrangement for the square plate with two opposite edges hard simply-supported (SS2) and the other two free or soft simply-supported (SS1)

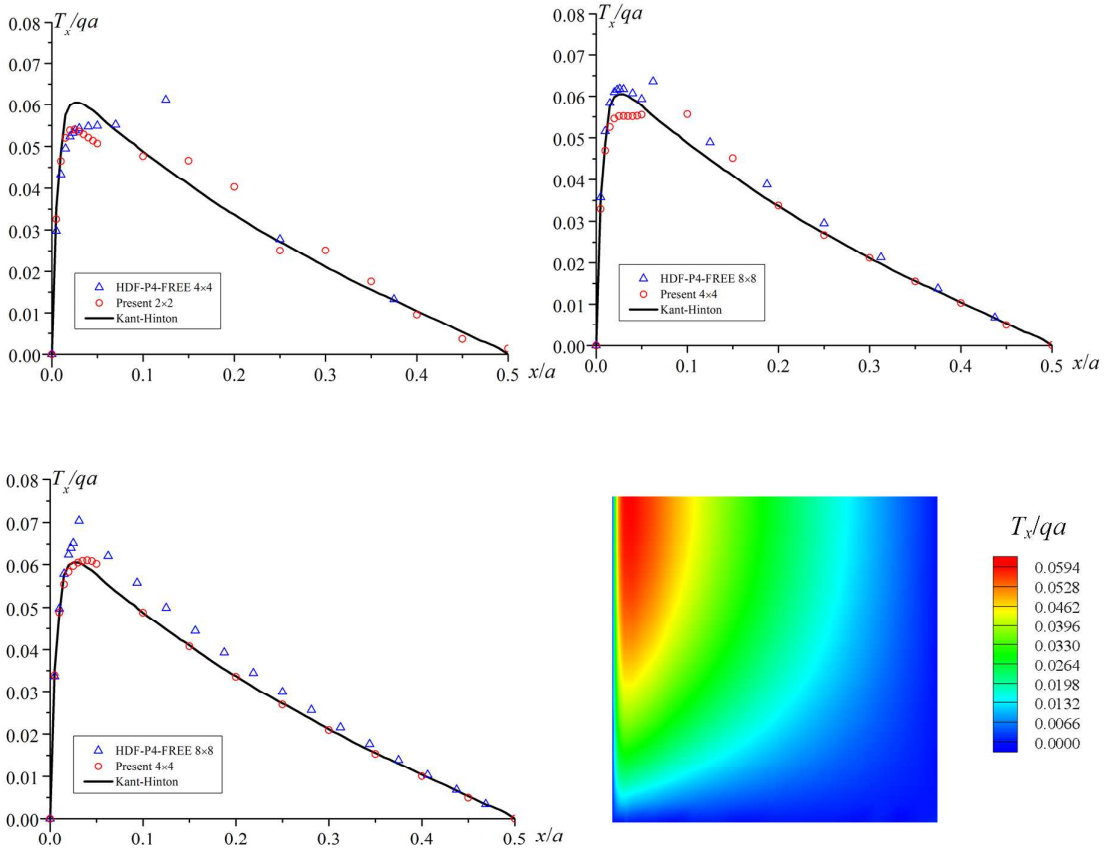

a) Distributions of the shear force T_x along the symmetric edge CD (y=0.5a) with mesh i) 2×2; ii) 4×4; iii) 8×8; and iv) convergent contour plot with mesh 8×8

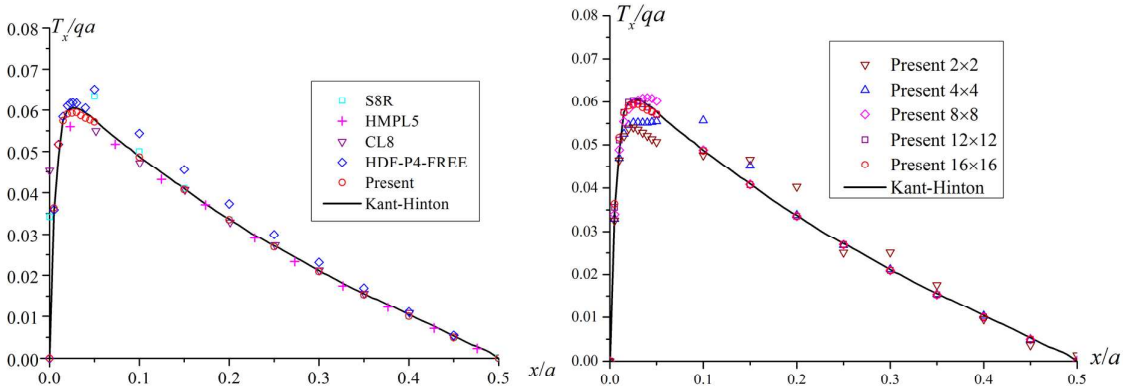

b) i) Comparisons of distributions of the shear force T_x along the symmetric edge CD (y=0.5a) with other methods with mesh 10×10; ii) Convergence of the present method

Figure 15. Distributions, contour plots and comparisons of the shear force T_x for the SFSF case

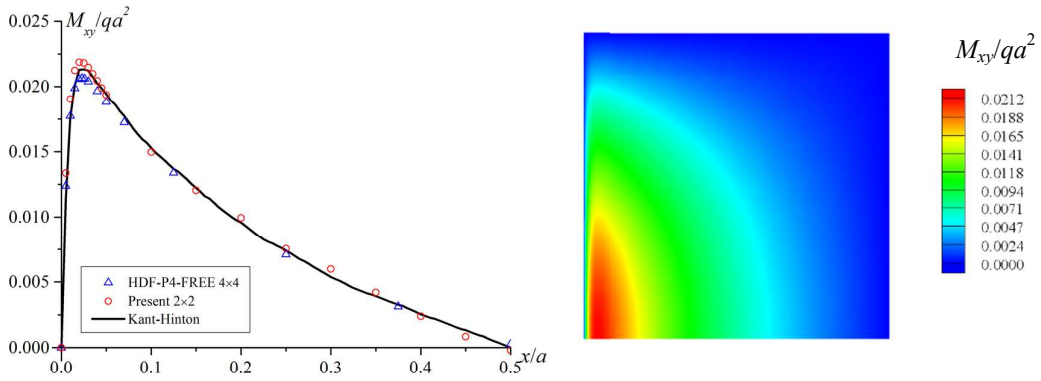

a) i) Distributions of the twisting moment M_{xy} along the hard simply-supported edge AB (y=0) with mesh 2×2; ii) Convergent contour plot with mesh 8×8

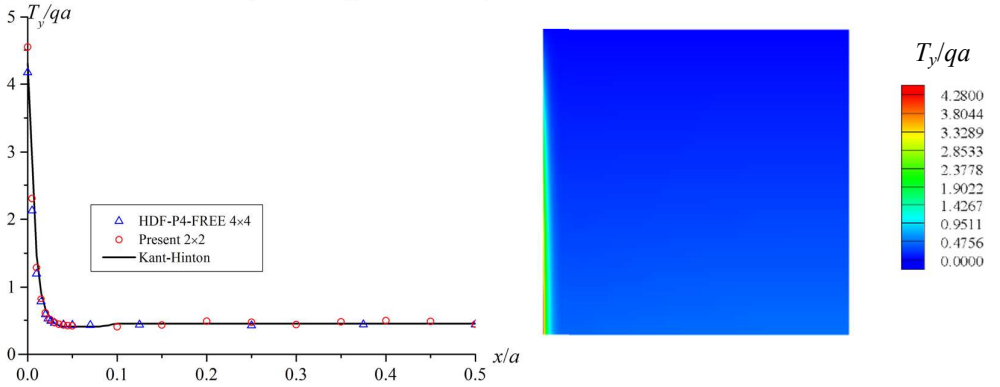

b) i) Distributions of the shear force T_y along the hard simply-supported edge AB (y=0) with mesh 2×2; ii) Convergent contour plot with mesh 8×8

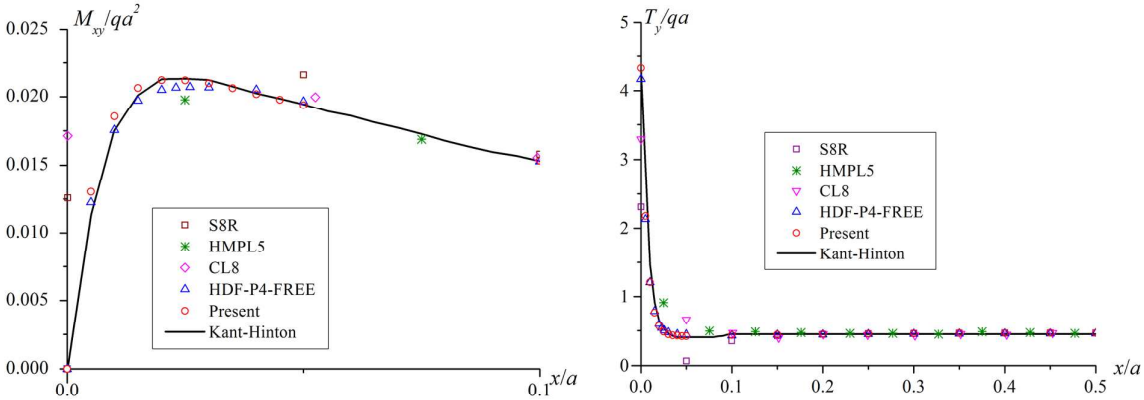

c) i) Comparisons of distributions of the twisting moment M_{xy} ; ii) Comparisons of distributions of the shear force T_y along the hard simply-supported edge AB (y=0) with mesh 10×10

Figure 16. Distributions, contour plots and comparisons of the twisting moment M_{xy} and the shear force T_y for the SFSF case

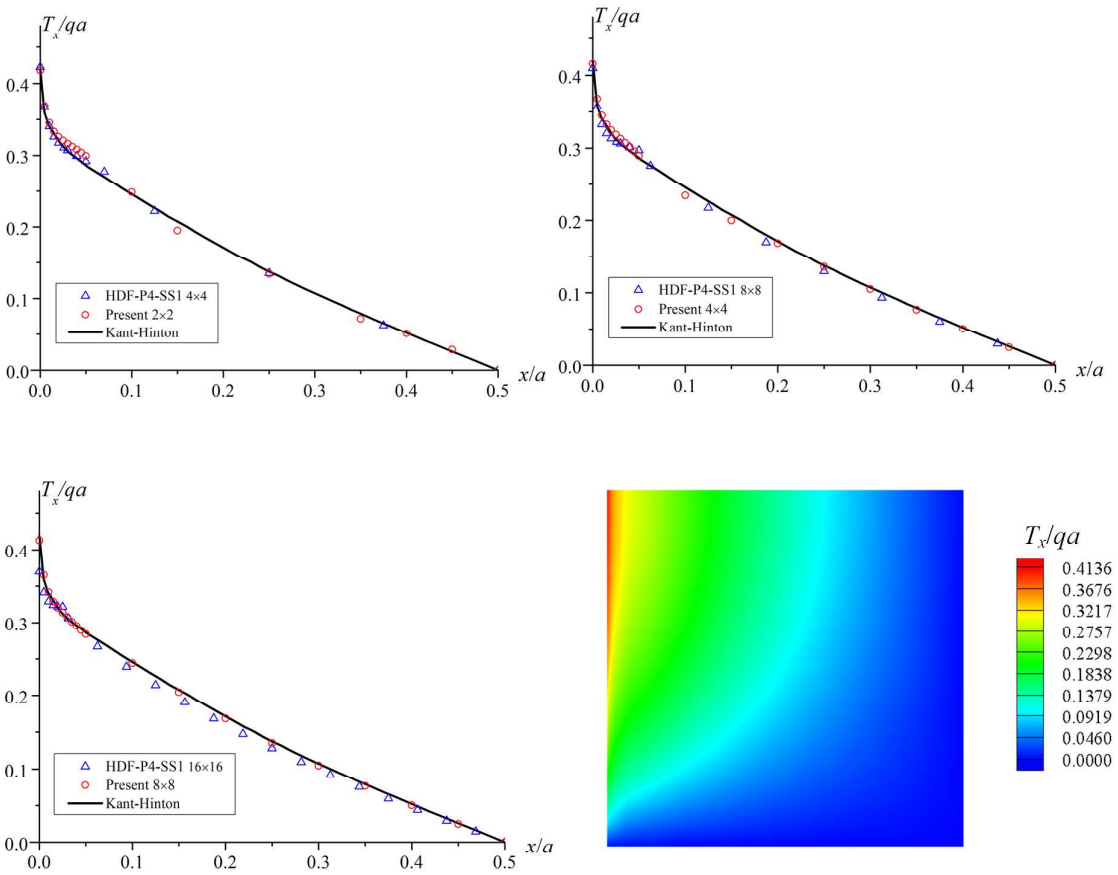

a) Distributions of the shear force T_x along the symmetric edge CD (y=0.5a) with mesh i) 2×2; ii) 4×4; iii) 8×8; and iv) convergent contour plot with mesh 8×8

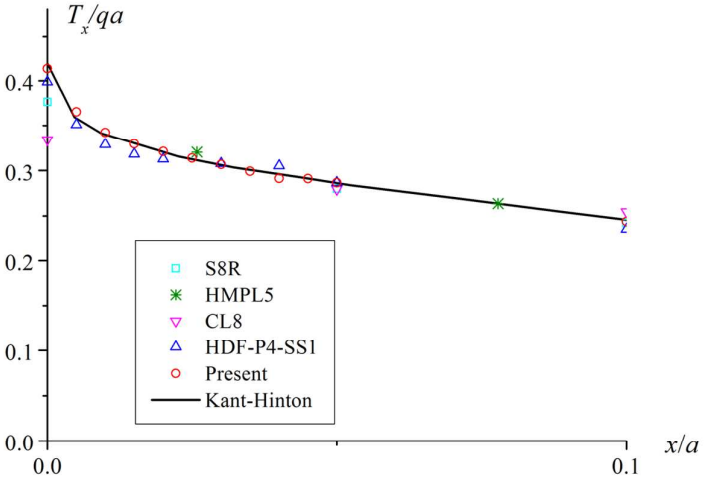

b) Comparisons of distributions of the shear force T_x along the symmetric edge CD (y=0.5a) the with other methods with mesh 10×10

Figure 17. Distributions, contour plots and comparisons of the shear force T_x for the SS*SS* case

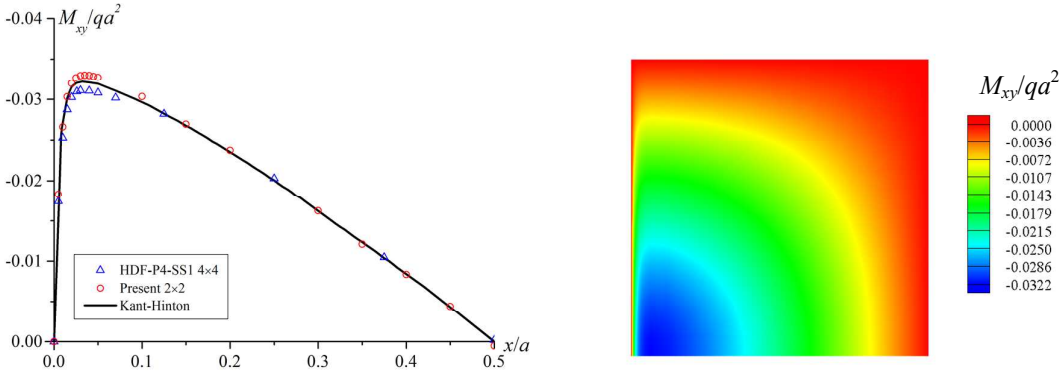

a) i) Distributions of the twisting moment M_{xy} along the hard simply-supported edge AB (y=0) with mesh 2×2; ii) Convergent contour plot with mesh 8×8

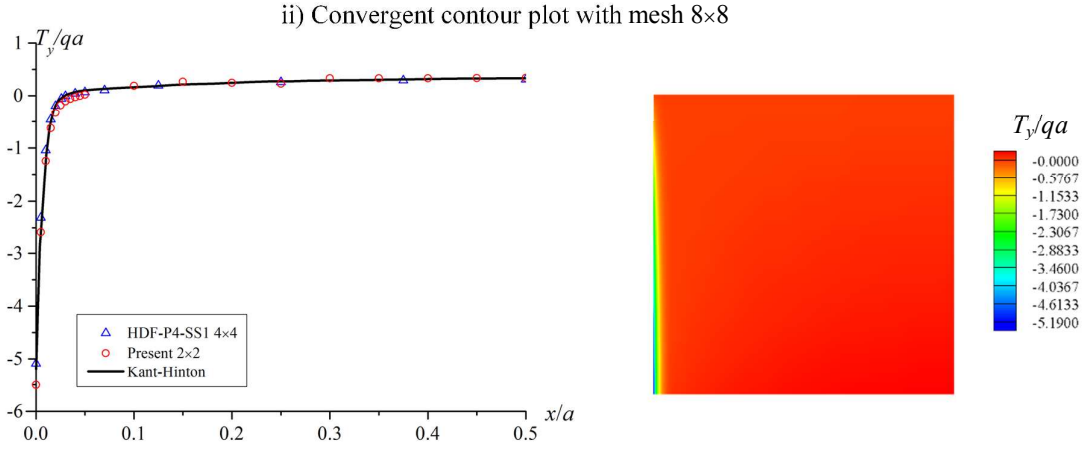

b) i) Distributions of the shear force T_y along the hard simply-supported edge AB (y=0) with mesh 2×2; ii) Convergent contour plot with mesh 8×8

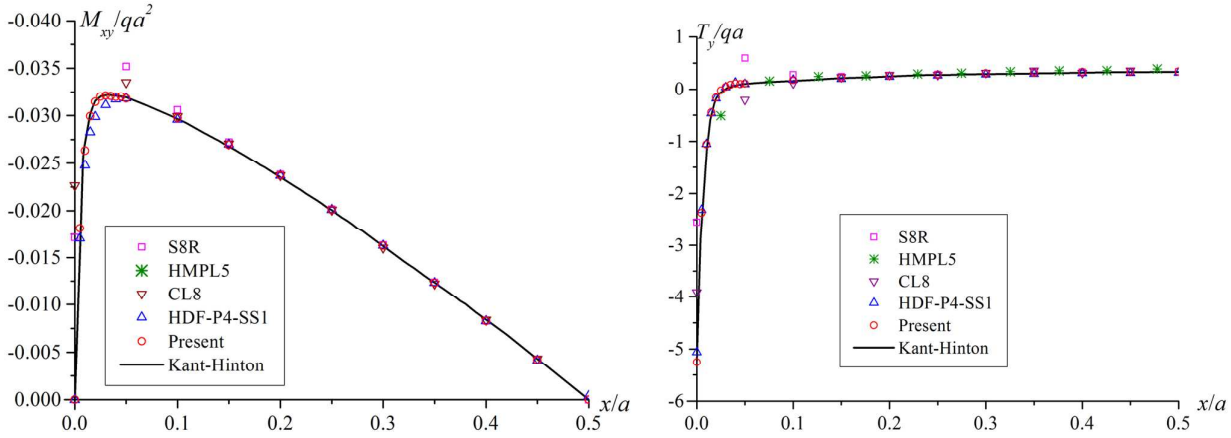

c) i) Comparisons of distributions of the twisting moment M_{xy} ; ii) Comparisons of distributions of the shear force T_y along the hard simply-supported edge AB (y=0) with mesh 10×10

Figure 18. Distributions, contour plots and comparisons of the twisting moment M_{xy} and the shear force T_y for the SS*SS* case